








# The structure of the high-affinity nickel-binding site in the Ni,Zn-HypA•UreE<sub>2</sub> complex

Barbara Zambelli <sup>1</sup>, Priyanka Basak <sup>2</sup>, Heidi Hu<sup>2</sup>, Mario Piccioli <sup>3</sup>, Francesco Musiani <sup>1</sup>, Valquiria Broll<sup>1</sup>, Lionel Imbert<sup>4</sup>, Jerome Boisbouvier <sup>4</sup>, Michael J. Maroney <sup>2,\*</sup> and Stefano Ciurli <sup>1,3,\*</sup>

<sup>1</sup>Laboratory of Bioinorganic Chemistry, Department of Pharmacy and Biotechnology, University of Bologna, Bologna, Italy, <sup>2</sup>Department of Chemistry and Program in Molecular and Cellular Biology, University of Massachusetts, Amherst, MA, USA, <sup>3</sup>Centre for Magnetic Resonance, Department of Chemistry, University of Florence, Florence Italy and <sup>4</sup>Univ. Grenoble Alpes, CNRS, CEA, Institut de Biologie Structurale (IBS), Grenoble, France

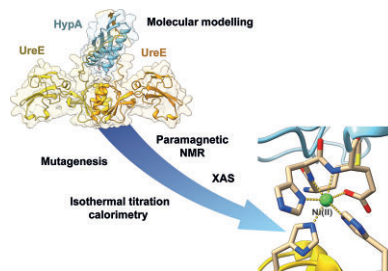
\*Correspondence: Department of Chemistry and Program in Molecular and Cellular Biology, University of Massachusetts, Amherst, MA, USA. E-mail: [mmaroney@chemistry.umass.edu](mailto:mmaroney@chemistry.umass.edu); E-mail: [stefano.ciurli@unibo.it](mailto:stefano.ciurli@unibo.it)

## Abstract

The maturation pathway for the nickel-dependent enzyme urease utilizes the protein UreE as a metallochaperone to supply Ni(II) ions. In *Helicobacter pylori* urease maturation also requires HypA and HypB, accessory proteins that are commonly associated with hydrogenase maturation. Herein we report on the characterization of a protein complex formed between HypA and the UreE<sub>2</sub> dimer. Nuclear magnetic resonance (NMR) coupled with molecular modelling show that the protein complex apo, Zn-HypA•UreE<sub>2</sub>, forms between the rigorously conserved Met-His-Glu (MHE motif) Ni-binding N-terminal sequence of HypA and the two conserved His102A and His102B located at the dimer interface of UreE<sub>2</sub>. This complex forms in the absence of Ni(II) and is supported by extensive protein contacts that include the use of the C-terminal sequences of UreE<sub>2</sub> to form additional strands of  $\beta$ -sheet with the Ni-binding domain of HypA. The Ni-binding properties of apo, Zn-HypA•UreE<sub>2</sub> and the component proteins were investigated by isothermal titration calorimetry using a global fitting strategy that included all of the relevant equilibria, and show that the Ni,Zn-HypA•UreE<sub>2</sub> complex contains a single Ni(II)-binding site with a sub-nanomolar  $K_D$ . The structural features of this novel Ni(II) site were elucidated using proteins produced with specifically deuterated amino acids, protein point mutations, and the analyses of X-ray absorption spectroscopy, hyperfine shifted NMR features, as well as molecular modeling coupled with quantum-mechanical calculations. The results show that the complex contains a six-coordinate, high-spin Ni(II) site with ligands provided by both component proteins.

**Keywords:** enzyme maturation, *Helicobacter pylori*, metallochaperone, nickel trafficking

## Graphical abstract



Models of the HypA•UreE<sub>2</sub> protein complex (A) and novel Ni(II) site (B) formed at the interface.

## Introduction

HypA is a monomeric metallochaperone that is generally associated with Ni(II) incorporation into the large subunit of [Ni,Fe]-hydrogenases,<sup>1–4</sup> while the dimeric UreE<sub>2</sub> serves this nickel transport function in bacteria that produce urease.<sup>4–9</sup> In *Helicobacter pylori* (*Hp*), HypA serves both functions in that HypA is also required for urease Ni(II) incorporation under physiological conditions.<sup>4,10–13</sup> *Hp* is a human pathogen that infects the stomach and is a major cause of ulcers, gastric cancers, and mucosa-associated

lymphoid tissue lymphoma.<sup>4,14,15</sup> Its ability to survive the acidic environment of the stomach depends on the activity of urease, a nickel-dependent enzyme that catalyzes the hydrolysis of urea to ammonia and CO<sub>2</sub> and thereby helps *Hp* maintain its internal pH as well as modify the pH of its environment.<sup>16</sup> Although [Ni,Fe]-hydrogenase is not required for acidic survival,<sup>17</sup> it is involved in utilization of H<sub>2</sub> as a source of energy and is associated with the virulence of the organism in terms of its ability to colonize gastric mucosa and to induce cancer.<sup>4,18,19</sup>

The activity of urease is partly controlled by Ni(II) insertion, as *Hp* expresses the urease protein under neutral conditions, but it remains largely apo-protein until the organism experiences acid shock, which results in rapid nickelation of the enzyme.<sup>16,20</sup> Numerous studies have shown that mutations that lead to defective nickel trafficking to urease (HypA/B or UreE<sub>2</sub> deletion, or interfere with the ability of HypA or UreE<sub>2</sub> to function as a nickel metallochaperone) lead to strains of *Hp* that are unable to survive acidic conditions,<sup>10,12,13,21–23</sup> as well as to inactive H<sub>2</sub>ase.<sup>17</sup> Thus, interfering with urease nickel incorporation provides a novel antibacterial strategy for treating *Hp* infections, including the growing number of clarithromycin-resistant infections.<sup>24</sup>

Recent work has shown that HypA and UreE<sub>2</sub> form a 1:1 protein complex that contains a single high-affinity nickel-binding site.<sup>25</sup> The work described here is focused on characterizing the Ni-binding properties of the HypA•UreE<sub>2</sub> complex and the structure of the novel Ni(II) site. Isothermal titration calorimetry (ITC) studies employing a global fitting strategy show that the affinity of this site ( $K_D \sim 10^{-10}$  M) is much tighter than typical for metallochaperones ( $K_D \sim \mu\text{M}$ )<sup>26</sup> and is more characteristic of Ni-responsive transcriptional regulators, such as InrS ( $K_D \sim 10^{-10}$  M)<sup>27</sup> or NikR ( $K_D \sim 10^{-8}$  M).<sup>28</sup> This tight Ni binding, as well as the strong interactions between HypA and UreE<sub>2</sub>, allowed for the isolation and characterization of the Ni,Zn-HypA•UreE<sub>2</sub> complex and three protein mutants.

X-ray-absorption spectroscopy (XAS) performed on isolated Ni-HypA•UreE<sub>2</sub> reveals a six-coordinate Ni(II) center containing three His residues. This six-coordinate Ni(II) site also gives rise to well-defined hyperfine-shifted resonances in the <sup>1</sup>H-NMR (nuclear magnetic resonance) spectrum. Detailed analysis of this NMR spectrum employing amino acid modifications of both UreE<sub>2</sub> and HypA, as well as proteins produced with specifically deuterated amino acids, reveals a structure that involves coordination of Ni(II) by His residues from both proteins (His102A and His102B from UreE<sub>2</sub>, and His2 from HypA), provides evidence regarding the remaining three ligands, proposes a model for the structure of the HypA•UreE<sub>2</sub> complex, and suggests a mechanism for coordination of Ni,Zn-HypA by UreE<sub>2</sub>. Density functional theory (DFT)-based computational studies corroborate the experimental results, yielding experimentally supported models for the Ni site in HypA as well as in the HypA•UreE<sub>2</sub> complex.

## Materials and methods

### Protein production

Wild-type (WT) HypA and its mutant L2\*HypA, where a Leu residue was inserted between the N-terminal Met1 and the His2 residue, were produced by modifying a previously reported protocol (see Supplementary Information).<sup>23</sup> WT HypA containing perdeuterated methionine or histidine was produced with the same protocol, using a modified M9 medium (12 g/L Na<sub>2</sub>HPO<sub>4</sub>, 6 g/L KH<sub>2</sub>PO<sub>4</sub>, 1 g/L NaCl); when OD<sub>600</sub> = 0.6 was reached, 0.16 mM of (2,3,3,4,4-D<sub>5</sub>, methyl-D<sub>3</sub>, 98%)-L-methionine (Cambridge Isotope Laboratories, MA, USA) or (2,3,3-D<sub>3</sub>, ring-D<sub>2</sub>, 98%)-L-histidine (Eurisotop, Saint Aubin, France) was added to the cellular growth medium and incubated at 25 °C for 1 h before adding 10 μM ZnSO<sub>4</sub> and IPTG (Isopropyl β-D-1-thiogalactopyranoside) as described in the procedure provided in the Supplementary Information.

A cell-free expression protocol was applied to produce HypA containing perdeuterated aspartate or glutamate. The sequence corresponding to *hypA* was cloned into a *pIVEX 2.3d* vector; in particular, the *pIVEX 2.3d* vector was PCR amplified using the primers 5'-gtcga**ctc**gagcgagctcc-3' and 5'-atgtg**catatg**tatatctctcttaaag-3', which contain the sequences (bold characters) for XhoI and NdeI,

respectively. The obtained sequence was digested with these restriction enzymes and ligated to the sequence of *hypA* obtained by restriction of *pET22b-hypA* with the same endonucleases.<sup>29</sup> Positive clones for *pIVEX 2.3d-hypA* were identified by colony PCR, restriction tests and sequencing on both strands. The recombinant plasmid was purified using the Nucleobond Xtra Maxi plus kit (Macherey-Nagel). The protein was synthesized *in vitro* using a cell-free expression system (ISBG, Grenoble). HypA was expressed under RNase-free conditions in dialysis mode, in a volume of 15 mL with a 1/10 ratio of reaction mixture to feeding mixture, for 16 h at 27 °C under gentle agitation. The cell-free mixture<sup>30</sup> contained 16 μg/mL of *pIVEX 2.3d-hypA*, 1 mM of 19 essential protonated amino acids, 0.8 mM of each rNTPs (guanosine-, uracil-, and cytidine-5'-triphosphate), 55 mM HEPES (4-(2-hydroxyethyl)-1-piperazineethanesulfonic acid) (pH 7.5), 68 μM folic acid, 0.64 mM cyclic adenosine monophosphate, 3.4 mM dithiothreitol, 27.5 mM ammonium acetate, 2 mM spermidine, 80 mM creatine phosphate, 200 mM potassium acetate, 18 mM magnesium acetate, 250 μg/mL creatine kinase, 27 μg/mL T7 RNA polymerase, 0.175 μg/mL tRNA, 5 μM ZnSO<sub>4</sub> and 400 μL/mL S30 *E. coli* bacterial extract. The latter was previously treated with 20 mM NaBH<sub>4</sub>, 20 mM D-malate and 20 mM amino-oxy-acetate to inhibit transaminase activity. The HypA samples containing <sup>2</sup>H-Glu and <sup>2</sup>H-Asp were prepared with the addition of 1 mM (2,3,3,4,4-D<sub>5</sub>, 98%)-L-glutamic acid or (2,3,3-D<sub>3</sub>, 98%)-L-aspartic acid, respectively. In both cases, the reaction mixture was clarified after incubation by centrifugation for 20 min at 15 000 ×g and 4 °C. The supernatant was diluted to 45 mL in 20 mM TrisHCl buffer at pH 7.5 containing 20 mM NaCl and 1 mM TCEP, and then loaded onto a RESSOURCE-Q 6 mL column (GE Healthcare) pre-equilibrated with 20 mM TrisHCl buffer at pH 7.2, containing 20 mM NaCl and 1 mM TCEP (tris(2-carboxyethyl)phosphine). The column was washed using a flow rate of 4 mL min<sup>-1</sup> with the starting buffer until the baseline was stable. A linear gradient of NaCl (220 mL, from 0.02 to 0.6 M) was applied to the column and the fractions containing HypA were combined, concentrated using 3 kDa ultra-filtration units (Millipore) to a final volume of 2 mL, and loaded onto a Superdex 75 10/300GL column equilibrated with 20 mM HEPES at pH 7.2, containing 200 mM NaCl and 1 mM TCEP for a final purification step. The fractions containing the purified protein, evaluated using SDS-PAGE, were pooled together, concentrated with Amicon Ultra concentrators (Millipore, GE) with a 3 kDa cutoff, and stored at -80 °C until use.

The protein-protein complexes were prepared starting from the single apo, Zn-HypA and UreE<sub>2</sub> or their mutants, mixing the components in equimolar amounts. Following addition of one equivalent of Ni(II), the samples were kept at room temperature for 2 h before loading the reaction mixture onto a Superdex S75 10/300 (GE Healthcare) size exclusion chromatographic column. The fractions containing the purified complexes were pooled together, concentrated with Amicon Ultra concentrators (Millipore, GE) with a 3 kDa cutoff, and stored at -80 °C until use.

The purity and integrity of UreE<sub>2</sub> and HypA containing deuterated amino acids were tested using mass spectrometry (EMBL Proteomics Core Facility, [https://www.embl.de/proteomics/proteomics\\_services/](https://www.embl.de/proteomics/proteomics_services/)). The absence of Ni in the purified apo-proteins was established using inductively coupled plasma optical emission spectrometry (ICP-OES), as previously described.<sup>31</sup>

### Size exclusion chromatography/multiple angle light scattering

The oligomerization properties of the single HypA and UreE<sub>2</sub> proteins and their complexes were investigated using size

exclusion chromatography (SEC) coupled with multiple angle light scattering (MALS). SEC-MALS measurements were performed using an Agilent HPLC with a Superdex 75 10/300 GL column (GE Healthcare) connected downstream to a multi-angle laser light scattering (MALS, at 690.0 nm) DAWN EOS (Wyatt Technology) photometer and to a 90° angle quasi-elastic (dynamic) light scattering (QELS) device (Wyatt Technology). The concentration of the eluted protein was determined using a refractive index detector (Optilab DSP, Wyatt). All experiments were performed at room temperature, with the system equilibrated with 20 mM HEPES pH 7.2 and 200 mM NaCl at 0.6 mL/min. Single protein samples consisted of 200  $\mu$ L of 130  $\mu$ M Ni,Zn-HypA, 130  $\mu$ M Ni,Zn-L2\*HypA, 45  $\mu$ M Ni-UreE<sub>2</sub>, 45  $\mu$ M Ni-H152A-UreE<sub>2</sub> and 45  $\mu$ M Ni-H102K-UreE<sub>2</sub>. The samples of protein complexes (100  $\mu$ L, 85  $\mu$ M) were prepared by mixing equimolar amounts of each protein prior to injection into the SEC column. All data were analysed using the ASTRA 4.90.07 software (Wyatt Technology), following the manufacturer's instructions.

### Isothermal titration calorimetry

The thermodynamics of the interaction among HypA, UreE<sub>2</sub>, and Ni(II) were investigated using isothermal titration calorimetry (ITC). Titrations were performed using a high-sensitivity VP-ITC microcalorimeter (MicroCal LLC, MA, USA.) at 25 °C in 20 mM HEPES, pH 7.2, 200 mM NaCl. The reference cell was filled with MilliQ water. The solutions containing the single proteins or their mutants (20–40  $\mu$ M) were loaded into the sample cell (1.4093 mL). Solutions (0.250 to 1.5 mM) of NiCl<sub>2</sub>, apo, Zn-HypA, apo, Zn-L2\*HypA, Ni,Zn-HypA or Ni,Zn-L2\*HypA in the same buffer were added (60 injections of 5  $\mu$ L) using a computer-controlled microsyringe. Control experiments were carried out by titrating the same solutions into buffer alone, under identical conditions, verifying that the heat of dilution was negligible.

The integrated heat data obtained for each titration were fitted using a nonlinear least-squares minimization algorithm to a theoretical titration curve, using the AFFINImeter software and a global fitting approach.<sup>32</sup> The used fitting model initially involved independent sites for simple equilibria, whereas the stoichiometric equilibria approach was used for the global fitting procedure. The  $\Delta H$  (reaction enthalpy change, cal mol<sup>-1</sup>) and  $K_a$  (binding constant, M<sup>-1</sup>) were the thermodynamic fitting parameters. The parameters  $r_M$  (scaling parameter for the protein concentration) and  $Q_{dil}$  (heat of dilution, cal mol<sup>-1</sup>) were also adjusted as fitting parameters. The reaction entropy was calculated using the relationships  $\Delta G = -RT \ln K_a$  ( $R = 1.9872$  cal mol<sup>-1</sup> K<sup>-1</sup>,  $T = 298$  K) and  $\Delta G = \Delta H - T\Delta S$ . A global fitting analysis was performed for the curves representing the titrations involving three species [HypA, UreE<sub>2</sub> and Ni(II)]. The statistical GoF (goodness of fit) parameter was used to obtain the best fit.

### X-ray absorption spectroscopy

The coordination environment of Ni(II) in the HypA-UreE<sub>2</sub> complex was monitored using X-ray absorption spectroscopy (XAS). Samples of each protein were rapidly buffer exchanged using a Zeba Spin Desalting column, 7 kDa MWCO (molecular weight cut-off, ThermoScientific) pre-equilibrated with NTP buffer (20 mM HEPES, 100 mM NaCl, 100 mM KCl, 5 mM MgCl<sub>2</sub>, 1 mM TCEP) at pH 7.2 or 6.3. Each protein was further diluted to working concentrations of 100–300  $\mu$ M in NTP buffer at the target pH prior to metal additions. A nickel acetate [Ni(OAc)<sub>2</sub>] stock solution (500 mM) was prepared in distilled and deionized water, and then further diluted to 9 mM working stock in NTP buffer at pH 7.2 or 6.3. The Ni(II) concentration in each stock solution was then ac-

curately determined by ICP-OES as previously described.<sup>23</sup> Ni,Zn-HypA•UreE<sub>2</sub> complexes at pH 7.2 or 6.3 were prepared by mixing equal molar equivalents of UreE<sub>2</sub> with Ni,Zn-HypA (after excess metals were removed by Chelex treatment) at each respective pH. Complexes were prepared with each protein at target concentrations between 100 and 300  $\mu$ M and equilibrated at room temperature for 30 minutes. Protein complexes were concentrated by spin filtration to approximately 100  $\mu$ L and then mixed with 400  $\mu$ L of NTP buffer at target pH, and then concentrated to target protein concentration of approximately 1 mM, and then mixed with 80% glycerol to a final glycerol concentration of 12%. The final flow through from spin filtration and a portion of each sample was reserved for protein and metal analyses (by ICP-OES) and found to contain nearly equal molar ratios of Ni and Zn. The sample prepared at pH 7.2 was found to contain 0.90 mM Ni and 0.85 mM Zn (Ni: Zn = 1: 0.94). The sample prepared at pH 6.3 was found to contain 0.75 mM Ni and 0.77 mM Zn (Ni: Zn = 1:1.03). The Ni,Zn-HypA•UreE<sub>2</sub> complexes were loaded into Kapton-taped polycarbonate sample holders and flash frozen with liquid N<sub>2</sub>. Samples were stored at -80 °C prior to data collection.

XAS data on the frozen samples were collected at the Stanford Synchrotron Radiation Lightsources (SSRL) at the SLAC National Accelerator Laboratory using dedicated ring conditions (3 GeV and 450–500 mA) on beamline 9-3 with a Si (220) double crystal monochromator. The frozen samples in polycarbonate holders with Kapton windows were immobilized on aluminum prongs and cooled to ~10 K using a liquid helium cryostat (Oxford Instruments). A 100 element Ge detector (Canberra) was used for collecting X-ray fluorescence data. To minimize scattering, a 3  $\mu$ m Z-1 filter and Soller slits were installed between the detector and sample. X-ray fluorescence data on Ni K-edge of the Ni,Zn-HypA•UreE<sub>2</sub> complex were energy calibrated by concurrently collecting spectra of a Ni metal foil in transmission mode. Extended X-ray absorption fine structure (EXAFS) data were collected to 15k above the K-edge for both metals.

Data reduction and analyses were performed according to previously published procedures adjusted for Ni and Zn K-edge XAS data (see Supplementary Information).<sup>33</sup> The Artemis software program<sup>34</sup> with FEFF6 and IFEFFIT algorithm was used to generate and fit single and multiple-scattering paths for each data set as described previously (see Supplementary Information).<sup>6,23,35</sup> To compare the different models fit to the data set, IFEFFIT utilizes three goodness of fit parameters:  $\chi^2$ , reduced  $\chi^2$  and the R-factor (see Supplementary Information). In comparing different models, minimizing the R-factor and reduced  $\chi^2$  parameter, and reasonable values of  $\sigma^2$  were used to determine the models that best fit the data. The R-factor will generally improve with increasing number of adjustable parameters, while reduced  $\chi^2$  will go through a minimum and then increase, indicating that the model is overfitting the data. The resolution of the data ( $\pi/2\Delta k$ ) was determined using  $\Delta k$ -values of 12.5  $\text{\AA}^{-1}$  and 10.5  $\text{\AA}^{-1}$  for Zn and Ni, yielding resolution values of 0.13  $\text{\AA}$  and 0.15  $\text{\AA}$ , respectively.

### Nuclear magnetic resonance spectroscopy

The interaction of HypA, UreE<sub>2</sub> and Ni(II) was monitored using nuclear magnetic resonance (NMR) spectroscopy. Protein samples consisted of (i) 0.5 mM <sup>15</sup>N-labeled apo, Zn-HypA, (ii) 0.3 mM apo, Zn-HypA(<sup>15</sup>N)•UreE<sub>2</sub>(<sup>14</sup>N) complex, and (iii) the same complex added with one equivalent of Ni(II) in 20 mM HEPES buffer at pH 7.2, containing 200 mM NaCl, in 90% H<sub>2</sub>O and 10% D<sub>2</sub>O, in the absence and in the presence of TCEP. NMR spectra were obtained using a Bruker AVANCE 950 spectrometer, operating at the proton nominal frequency of 950.2 MHz (22.3 T)

and equipped with a 5 mm TCI-HCN z-gradient cryo-probe; the temperature was calibrated at 298 K. Due to the high salt concentration, shaped NMR tubes (Bruker BioSpin AG) were used to improve the signal-to-noise ratio during NMR data collection. The  $^1\text{H}$  chemical shifts were referenced to 2,2-dimethyl-2-silapentane-5-sulfonic acid sodium salt (DSS), while the  $^{15}\text{N}$  chemical shifts were referenced indirectly to DSS, using the ratios of the gyromagnetic constants. The  $^1\text{H}$ - $^{15}\text{N}$  HSQC spectra were recorded using spectral widths of 13297.872 Hz ( $^1\text{H}$ , 14.0 ppm) and 3852.080 Hz ( $^{15}\text{N}$ , 40.0 ppm) with maximal evolution times of 57.7 ms ( $^1\text{H}$ , 2048 points) and 16.6 ms ( $^{15}\text{N}$ , 256 points). All NMR spectra were processed using NMRpipe.<sup>36</sup> The original data were zero-filled (2048  $\times$  1024 points), a cosine-squared apodization function was applied in both dimensions, and a linear prediction algorithm was applied to the indirect dimension prior to Fourier transformation. The spectra were analysed using POKY.<sup>37</sup>

$^1\text{H}$ -NMR experiments tailored for the identification of hyperfine shifted and fast relaxing signals<sup>38</sup> were performed on an AVANCE 400 Bruker NMR spectrometer equipped with a 5 mm  $^1\text{H}$  selective probe and operating at 400.13 MHz  $^1\text{H}$  Larmor Frequency. Spectra were collected with the superWEFT pulse sequence, using 52 ms, 20 ms and 62 ms as acquisition, recovery, and inter-pulse delays, respectively. The spectral window was 156 kHz (390 ppm). The number of acquired scans ranged from 400 K to 800 K, and the experiment time was typically 16–48 h. Prior to Fourier transform, FIDs were multiplied by a cosine square weighting function followed by a 20 Hz Lorentzian line broadening. Phase and baseline correction were performed manually.

### Modeling of the Ni,Zn-HypA•UreE<sub>2</sub> complex

An initial model for the apo,Zn-HypA•UreE<sub>2</sub> complex, devoid of any metal ion, was calculated using ColabFold,<sup>39</sup> AlphaFold2,<sup>40</sup> and RoseTTAFold.<sup>41</sup> The best model was selected on the basis of predicted local-distance difference test (LDDT).<sup>42</sup> The Ni(II)-binding site at the HypA•UreE<sub>2</sub> interface was modelled on the protein complex achieved in the previous modelling step through a computational procedure already used to reconstruct the metal binding site in other proteins,<sup>43–45</sup> involving the use of the loop optimization routines available in Modeller.<sup>46</sup> The van der Waals parameters for Ni(II) were derived from the Zn(II) parameters included in the CHARMM22 force field<sup>47</sup> implemented in the Modeller v9.18 package by applying a scale factor of 1.12 calculated on the basis of the Ni(II) ionic radius. Constraints were imposed using a Gaussian-shaped energy potential for distances, angles and dihedrals, in order to correctly position the Ni(II) ions with respect to the experimentally identified ligated residues (see Results). During the loop optimization procedure, 500 models were generated. The best model was selected on the basis of the lowest value of the DOPE score included in Modeller.<sup>48</sup> Structural analyses were conducted using ProCheck,<sup>49</sup> UCSF Chimera,<sup>50</sup> and UCSF ChimeraX.<sup>51,52</sup>

### Modeling of the Ni-sites in Ni,Zn-HypA and in the Ni,Zn-HypA•UreE<sub>2</sub> complex

The starting structural model for the coordination sphere of Ni(II) in Ni,Zn-HypA•UreE<sub>2</sub> was built using the structure of the HypA-UreE<sub>2</sub> apo-protein complex that resulted from the previously described modelling stage. In particular, the N-terminal N atom of Met1, the amide and side chain imidazole N $\delta$ 1 atoms of His2, and the amide N and side chain carboxylate O $\epsilon$ 1 and O $\epsilon$ 2 atoms of Glu3 from HypA, together with the N $\epsilon$ 2 atoms of His102A and His102B from the homodimeric UreE<sub>2</sub>, were included in the model.

These selected residues were capped with a -CH<sub>3</sub> and a -NH<sub>2</sub> group at the N- and C-termini, respectively. A starting model of the Ni(II) site in Ni,Zn-HypA was then derived by removing the two histidine residues His102A and His102B from UreE<sub>2</sub>, and adding the HypA Met1 N-terminal N atom in the coordination sphere of the metal ion through the rotation of the protein backbone using UCSF Chimera.<sup>50</sup> A second starting model of the Ni(II) site in Ni,Zn-HypA was generated in the same way, but with the addition of a water molecule as the sixth ligand of the Ni(II) ion instead of Glu3 O $\epsilon$ 2. These three models were optimized using DFT computations, carried out using the program ORCA 4.0.1<sup>53</sup> and the Becke three-parameter hybrid functional combined with Lee–Yang–Parr correlation functional (B3LYP/G)<sup>54,55</sup> as defined in the Gaussian software.<sup>56</sup> All atoms except Ni(II) were described by the Pople-style 6–31(p, d) basis set with diffuse functions on all atoms.<sup>57</sup> The Ni(II) ion was described with the Los Alamos effective core potentials (LANL2DZ ECP).<sup>58</sup> TightSCF criteria for SCF [energy change  $<1.0 \times 10^{-8}$  atomic unit (au)] and standard criteria for the geometry optimization (energy change  $<5 \times 10^{-6}$  au, RMS gradient  $<1 \times 10^{-4}$  au, maximum element of gradient  $<3 \times 10^{-4}$  au, root mean square deviation (RMSD) displacement  $<2 \times 10^{-3}$  au, maximum displacement  $<4 \times 10^{-3}$  au) were used. Frequency computations were executed to determine the nature of the critical points. Supplementary Table SI-5 reports the Ni-ligand distances obtained for the calculated models.

## Results

### Protein and Ni(II) interactions by SEC–MALS

UreE<sub>2</sub> and HypA were expressed and purified as previously reported.<sup>5,23</sup> Mass spectrometry, performed on protein samples, confirmed that both proteins were purified as intact polypeptides, and no evidence of C-terminal protein degradation, which was reported in a previous work,<sup>23</sup> was observed for UreE<sub>2</sub>, in the absence or in the presence of TCEP. This result is consistent with SDS-PAGE under denaturing conditions, which presented a unique band at ca. 20 kDa, corresponding to the UreE monomer. In addition to studying the native proteins, the L2\*HypA mutant,<sup>23,25</sup> as well as the H102K-UreE and H152A-UreE variants,<sup>5</sup> in which residues known to be involved in Ni(II) binding were mutated, were also analysed to dissect the role of each metal binding residue for metal binding in the hetero-complex. The molecular mass of the Ni(II) complexes of UreE<sub>2</sub>, HypA, and of their mutants in solution was determined using a combination of SEC and MALS (Fig. 1).

The elution profile of the single proteins is consistent with the presence of a monomer for Ni,Zn-HypA and Ni,Zn-L2\*HypA (MW = 14.4 and 14.8 kDa respectively, theoretical mass of the monomer 13.2 kDa, Fig. 1A, B) and a dimer for Ni-UreE<sub>2</sub> and Ni-H102K-UreE<sub>2</sub> (MW = 38.7 and 42.4 kDa, theoretical mass of the monomer 19.5 kDa, Fig. 1A, C), confirming previously reported data for the WT proteins and showing that the two protein mutants possess the same oligomeric state in solution as the native proteins.<sup>5,23,25,59</sup> In contrast, Ni-H152A-UreE<sub>2</sub> eluted in two peaks, showing MW = 76.8 and 42.7 kDa (Fig. 1D). This indicates that, in this case, the presence of Ni(II) drives a protein tetramerization equilibrium in solution. SEC–MALS data obtained mixing equimolar amounts of Ni,Zn-HypA and UreE<sub>2</sub> showed the formation of a peak with a lower retention volume, corresponding to MW = 53.4 kDa, compatible with the interaction of one UreE<sub>2</sub> dimer with one HypA monomer (theoretical mass 52 kDa) (Fig. 1A). Such a Ni,Zn-HypA•UreE<sub>2</sub> complex is formed also when Ni,Zn-HypA is present in solution together with H152A-UreE<sub>2</sub> (Fig. 1D) or when UreE<sub>2</sub> is co-eluted in the presence of Ni,Zn-L2\*HypA (Fig. 1B), indicating

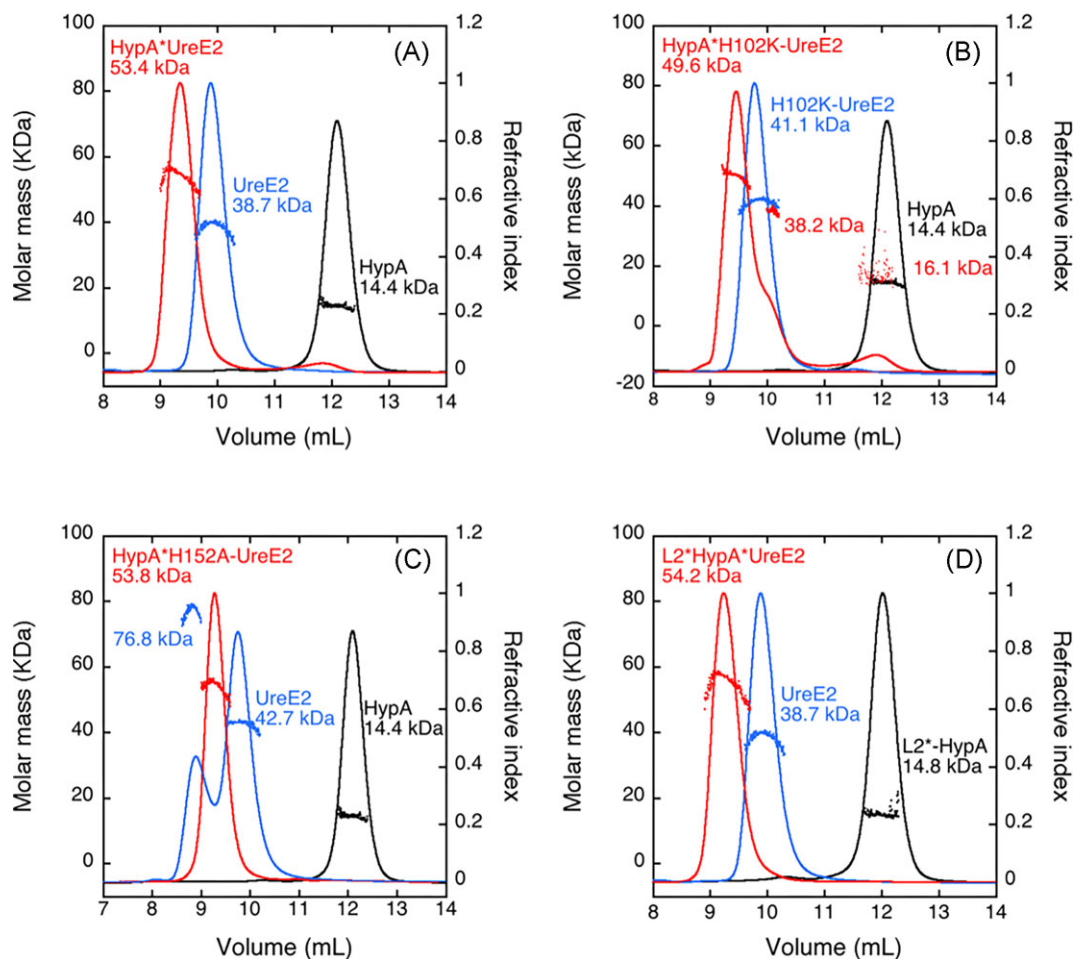


**Fig. 1.** Molar mass distribution plot for Ni,Zn-HypA, Ni-UreE<sub>2</sub> and Ni,Zn-HypA•UreE<sub>2</sub> (A) and their L2\*HypA (B), H102K-UreE<sub>2</sub> (C), and H152A-UreE<sub>2</sub> (D) mutants as derived from size exclusion chromatography (SEC) coupled with multiple angle light scattering (SEC-MALS). The solid lines indicate the traces from the refractive index detector after elution from SEC, and the dots are the weight-average molecular weights for each slice (measured every half second) as calculated from the MALS data.

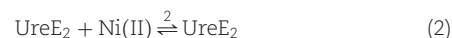
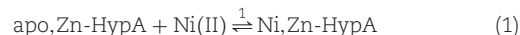
that both mutants maintain the ability to interact as the native proteins, in the presence of Ni(II). On the other hand, in the case of Ni,Zn-HypA co-eluted with the H102K-UreE<sub>2</sub> mutant, a complex chromatogram is observed (Fig. 1C) in which the prevalent species in solution corresponds to the Ni,Zn-HypA•H102K-UreE<sub>2</sub> complex (MW = 49.6 kDa), together with two additional peaks that correspond to the separate proteins. This indicates that the complex partially dissociates during elution, likely because of a decreased affinity of the protein-protein interaction caused by the H102K mutation.

### Examination of protein and Ni(II) interactions by ITC

All thermodynamic parameters obtained from ITC titrations are listed in Table 1. Ni(II) titration of either apo,Zn-HypA (Supplementary Fig. SI-1) or UreE<sub>2</sub> (Supplementary Fig. SI-2) produced an exothermic reaction, as indicated by negative peaks following each injection of Ni(II) (Supplementary Figs. SI-1A and SI-2A).

A fit of the integrated heat data (Supplementary Figs. SI-1B and SI-2B) using a single set of independent binding sites (Eqns. 1, 2) indicated the interaction of one Ni(II) ion per apo,Zn-HypA monomer ( $K_D = 0.90 \mu\text{M}$ ) and one Ni(II) ion per UreE<sub>2</sub> dimer ( $K_D = 0.29 \mu\text{M}$ ). In both cases, the enthalpic contribution is favorable, while the entropic contribution is positive for apo,Zn-HypA

binding and negative for UreE<sub>2</sub> binding. These results largely confirm the previously obtained thermodynamic parameters for Ni(II) titrations of apo,Zn-HypA<sup>25</sup> ( $K_D = 0.97 \mu\text{M}$ ) while they contrast with those obtained by Sun *et al.* on the same protein prepared using a different protocol<sup>59</sup> ( $K_D = 14 \mu\text{M}$ ). In the case of UreE<sub>2</sub>, the value obtained for the dissociation constant agrees with those obtained by Bellucci *et al.*<sup>5</sup> ( $K_D = 0.15 \mu\text{M}$ ) and by Yang *et al.*<sup>59</sup> ( $K_D = 0.53 \mu\text{M}$ ) while it differs by one order of magnitude with the value reported by Hu *et al.*<sup>25</sup> ( $K_D = 0.067 \mu\text{M}$ ), a discrepancy possibly caused by the slow protein degradation reported in the latter study.



Interaction of UreE<sub>2</sub> and apo,Zn-HypA in the absence of Ni(II) also occurs with an exothermic reaction (Supplementary Fig. SI-3A) whose thermodynamic parameters were obtained from the fit of the integrated heat to Eqn. 3 (Supplementary Fig. SI-3B, Table 1). The dissociation constant of this apo,Zn-HypA•UreE<sub>2</sub> complex ( $K_D = 0.84 \mu\text{M}$ ) confirmed the values previously obtained by Hu *et al.*<sup>23,25</sup> ( $K_D = 0.90 \mu\text{M}$ ) and Yang *et al.*<sup>59</sup> ( $K_D = 1.2 \mu\text{M}$ ).





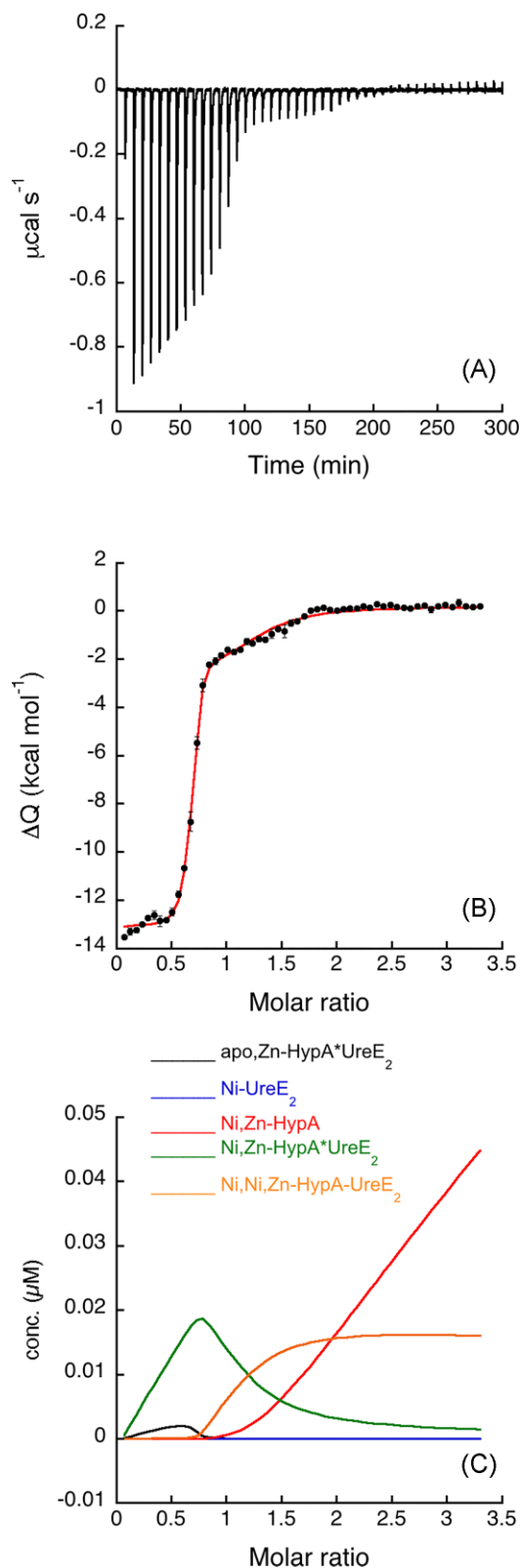


**Fig. 2.** Ni,Zn-HypA titration of UreE<sub>2</sub>. (A) Heat response for injections of 0.45 mM Ni,Zn-HypA into 30 μM UreE<sub>2</sub>. (B) Integrated heat data of the titration as a function of Ni,Zn-HypA/UreE<sub>2</sub> molar ratio. The continuous line represents the best fit (GoF = 58.8%) obtained with a model involving a global fit according to Eqn. 4. (C) Concentration distribution of the different species occurring during the titration described in (B), calculated using the thermodynamic parameters obtained from the fit and the binding model described by Eqn. 4.

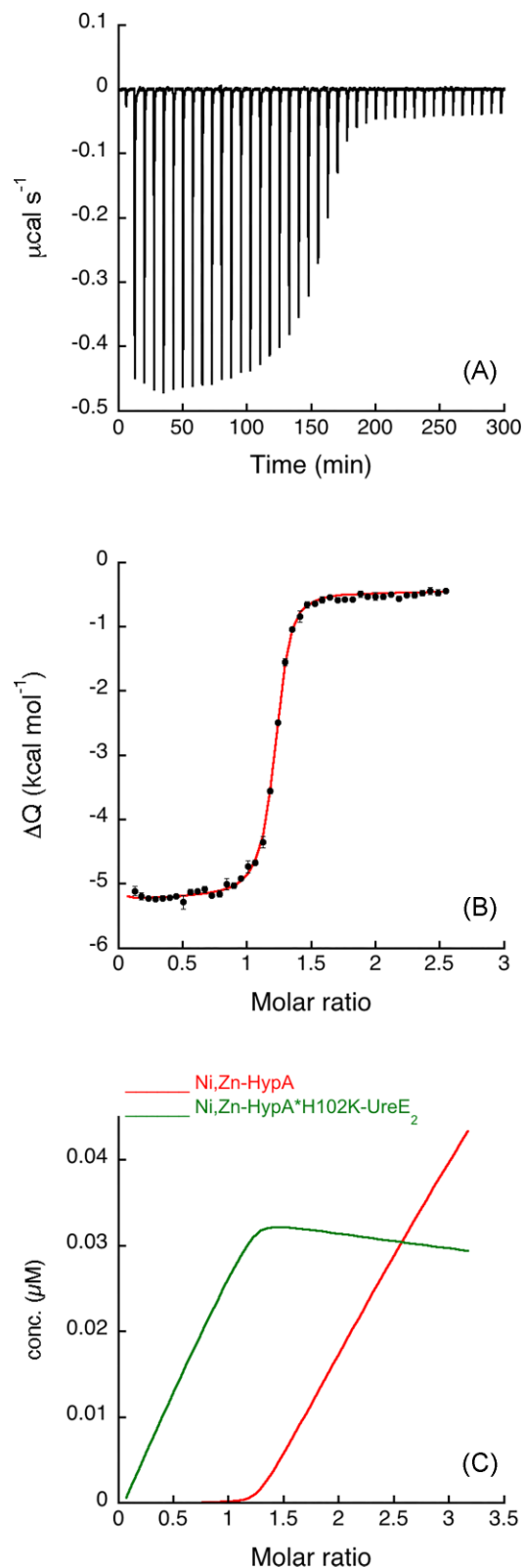
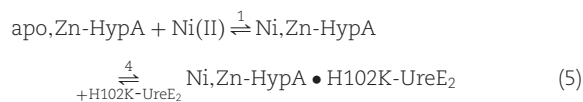


**Fig. 3.** Ni,Zn-HypA titration of H102K-UreE<sub>2</sub>. (A) Heat response for injections of 0.45 mM Ni,Zn-HypA into 30 μM H102K-UreE<sub>2</sub>. (B) Integrated heat data of the titration as a function of Ni,Zn-HypA/H102K-UreE<sub>2</sub> molar ratio. The continuous line represents the best fit (GoF = 68.4%) obtained with a model involving a global fit according to Eqn. 5. (C) Concentration distribution of the different species occurring during the titration described in (B), calculated using the thermodynamic parameters obtained from the fit and the binding model described by Eqn. 5.

The fit derived from these equilibria reproduced the integrated data well (Fig. 2B and Table 1). The dissociation constants of the binary complexes derived using this global fit are consistent with those obtained by fitting the single binding isotherms (Table 1), and additionally indicate the formation of two binding sites for Ni(II) in the protein complex, one with affinity in the sub-nanomole range ( $K_D = 0.15$  nM), which was not present in the separate proteins, and one with affinity in the sub-micromole range ( $K_D = 0.13$   $\mu$ M). A plot of species distribution as a function of the UreE<sub>2</sub>/apo,Zn-HypA molar ratio is reported in Fig. 2C.

To dissect the Ni(II) and protein binding events, and to investigate the roles of Ni(II) binding residues for the formation of the Ni(II) ternary complex, titrations were replicated with forms of UreE<sub>2</sub> and HypA in which known Ni(II) binding residues (His102 and His152 for UreE<sub>2</sub><sup>5</sup> and the N-terminus of HypA<sup>23</sup>) were mutated to obtain the H102K and H152A UreE<sub>2</sub> as well as the L2\*HypA (an insertion of Leu after the N-terminal Met residue) mutants. As previously reported,<sup>5</sup> Ni(II) titration of H102K-UreE<sub>2</sub> did not produce any heat of binding (Supplementary Fig. SI-4A), indicating of the absence of reaction under the experimental conditions. Similarly, apo,Zn-HypA titration of H102K-UreE<sub>2</sub> provided a very low reaction heat that did not significantly change with increasing molar ratio (Supplementary Fig. SI-4B), indicating that mutation of His102 has a detrimental effect on the protein-protein interaction when Ni(II) is not present in solution.

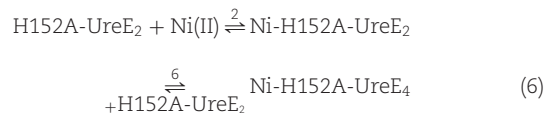
In contrast, Ni,Zn-HypA titration of the H102K-UreE<sub>2</sub> mutant produced an exothermic event (Fig. 3A), indicating that the presence of the Ni(II) ion in the system restores interactions between the two proteins. A global fit of the data, obtained using the AFFINImeter software as described earlier, was performed using a modified scheme (Eqn. 5) that considers two binding equilibria: (1) the apo,Zn-HypA interaction with Ni(II) and (4) the formation of the ternary complex with H102K-UreE<sub>2</sub>, while it does not include the single equilibria for Ni(II) binding to H102K-UreE<sub>2</sub> or for apo,Zn-HypA binding to H102K-UreE<sub>2</sub>, neither of which produced significant heats of binding (Supplementary Fig. SI-4). The global fitting procedure combined the isotherms for the interaction between HypA and Ni(II) (Supplementary Fig. SI-1) and that for the formation of the ternary complex, resulting in the fit shown in Fig. 3B.



The dissociation constant of the Ni,Zn-HypA complex thus derived is consistent with that obtained by fitting the single binding isotherm (Table 1). This fit additionally provides a value for the dissociation constant of the ternary complex ( $K_D = 60$  nM), which indicates that the H102K mutation decreases the affinity of the ternary complex for Ni(II) by  $\sim 400$  times.

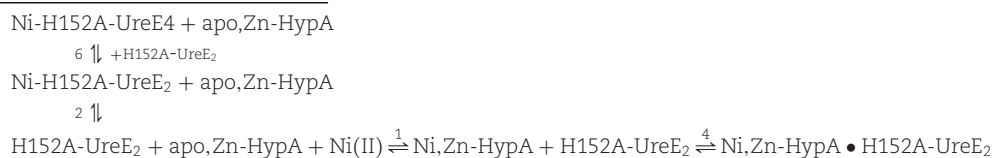
Similar experiments were conducted for the H152A-UreE<sub>2</sub> mutant. Titration of this protein with Ni(II) provides an exothermic binding (Supplementary Fig. SI-5A) as previously reported.<sup>5</sup> A fit

using a single site binding model provided the thermodynamic parameters  $K_D = 640 \pm 20$  nM,  $\Delta H_{\text{H152A-Ni}} = -6.93 \pm 0.03$  kcal mol<sup>-1</sup>,  $\Delta S_{\text{H152A-Ni}} = +5.09$  cal mol<sup>-1</sup> K<sup>-1</sup>, confirming previous values.<sup>5</sup> As this mutant was proven to undergo protein tetramerization upon Ni(II) binding using SEC-MALS experiments (*vide supra*), the fitting was performed including the dimer of dimer formation in the model (Eqn. 6).



A fit performed using this approach (Supplementary Fig. SI-5B) determined that Ni(II) binding to the H152A-UreE<sub>2</sub> mutant occurs (Table 1) with a dissociation constant  $K_D = 17$  nM, while protein dimerization features a dissociation constant one order of magnitude lower affinity ( $K_D = 0.909$   $\mu$ M). Substitution of His152 with an alanine residue in the H152A-UreE<sub>2</sub> mutant strongly decreases the protein affinity for apo,Zn-HypA (Supplementary Fig. SI-6): indeed, injections of apo,Zn-HypA into a H152A-UreE<sub>2</sub> solution generates a moderate thermal response that is observed as negative peaks following each injection. This effect does not decrease with the progress of the titration, indicating either a low interaction affinity (not sufficient to produce a binding isotherm) or a non-specific effect. The titration of the H152A-UreE<sub>2</sub> with Ni,Zn-HypA, on the other hand, revealed the restoration of protein-protein interactions, occurring with an exothermic reaction (Fig. 4A). A fit of the integrated heat data (Fig. 4B) was carried out using a model that considers all equilibria present in this solution (Eqn. 7): (1) Ni(II) binding to apo,Zn-HypA, (2) Ni(II) binding to H152A-UreE<sub>2</sub>, (4) Ni(II) binding to apo,Zn-HypA•H152A-UreE<sub>2</sub> complex, and (6) formation of the Ni-H152A-UreE<sub>4</sub> complex.

A good fit could be obtained only by fixing the affinity constants for the apo,Zn-HypA and of H152A-UreE<sub>2</sub> interactions with Ni(II) to the values provided by the single isotherms (Table 1). Although this procedure provides an interpolation curve (Fig. 4B) that is consistent with the experimental data, this suggests that some other event might occur during the titration, such as conformational change or protein aggregation, that was not considered. The dissociation constants obtained from the fit are  $K_D = 63$  nM and  $K_D = 0.62$   $\mu$ M for the Ni,Zn-HypA•H152A-UreE<sub>2</sub> and for the Ni-H152A-UreE<sub>4</sub> complexes, respectively. These values indicate that the affinity of the high-affinity binding site for Ni(II) decreases by two-orders of magnitude in the mutant ternary complex Ni,Zn-HypA•H152A-UreE<sub>2</sub> relative to the WT, as also observed for the analogous complex in the case of the H102K-UreE<sub>2</sub> mutant, the latter featuring similar affinity for Ni(II) as the H152A-UreE<sub>2</sub> mutant ( $K_D = 60$  nM, Table 1). The value for the Ni-UreE<sub>4</sub> dissociation constant is similar (0.62 vs. 0.91  $\mu$ M) to that obtained by directly titrating the H152A-UreE<sub>2</sub> mutant with Ni(II), indicating a good consistency of the analysis. The concentration distribution of the different species upon the increasing HypA/H152A-UreE<sub>2</sub> molar ratio is shown in Fig. 3C.







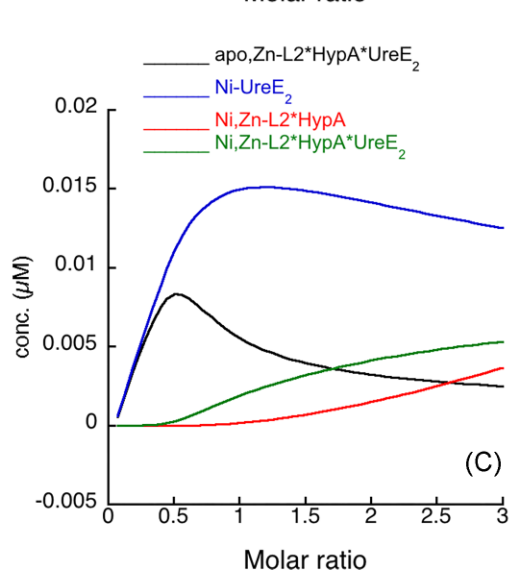
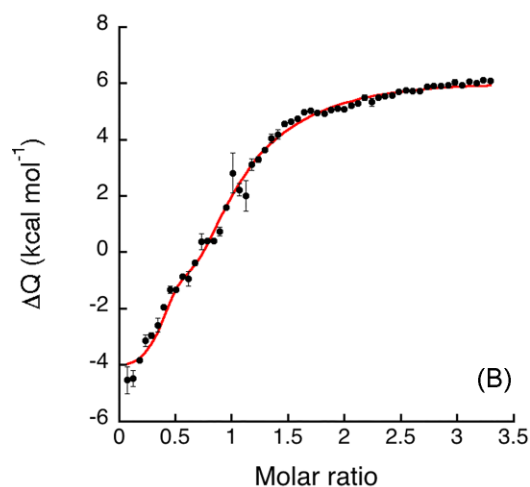
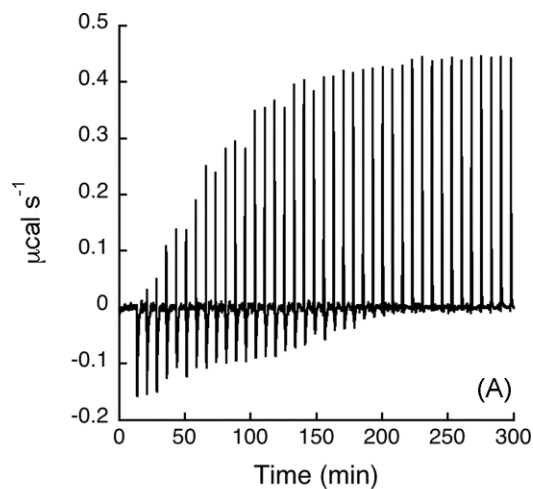
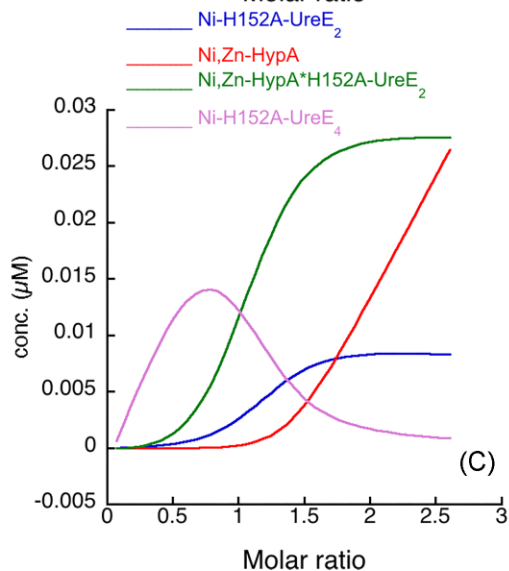
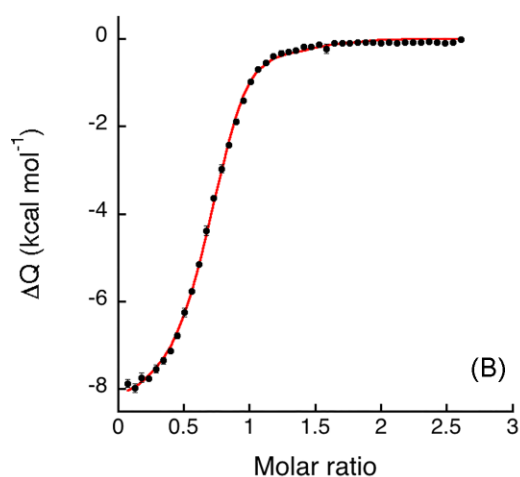
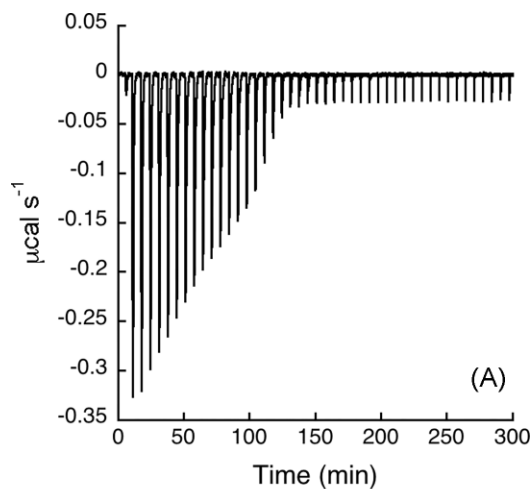


**Fig. 4.** Ni,Zn-HypA titration of H152A-UreE<sub>2</sub>. (A) Heat response for injections of 0.45 mM Ni,Zn-HypA into 30 μM H152A-UreE<sub>2</sub>. (B) Integrated heat data of the titration as a function of Ni,Zn-HypA/H152A-UreE<sub>2</sub> molar ratio. The continuous line represents the best fit (GoF = 58.4%) obtained with a model involving a global fit according to Eqn. 7. (C) Concentration distribution of the different species occurring during the titration described in (B), calculated using the thermodynamic parameters obtained from the fit and the binding model described in Eqn. 7.

**Fig. 5.** Ni,Zn-L2\*HypA titration of UreE<sub>2</sub>. (A) Heat response for injections of 0.412 mM apo, Zn-L2\*HypA into 27.5 μM UreE<sub>2</sub>. (B) Integrated heat data of the titration as a function of apo, Zn-L2\*HypA/UreE<sub>2</sub> molar ratio. The continuous line represents the best fit (GoF = 45.5%) obtained with a model involving a global fit according to Eqn. 8. (C) Concentration distribution of the different species occurring during the titration described in (B), calculated using the thermodynamic parameters obtained from the fit and the binding model described by Eqn. 8.

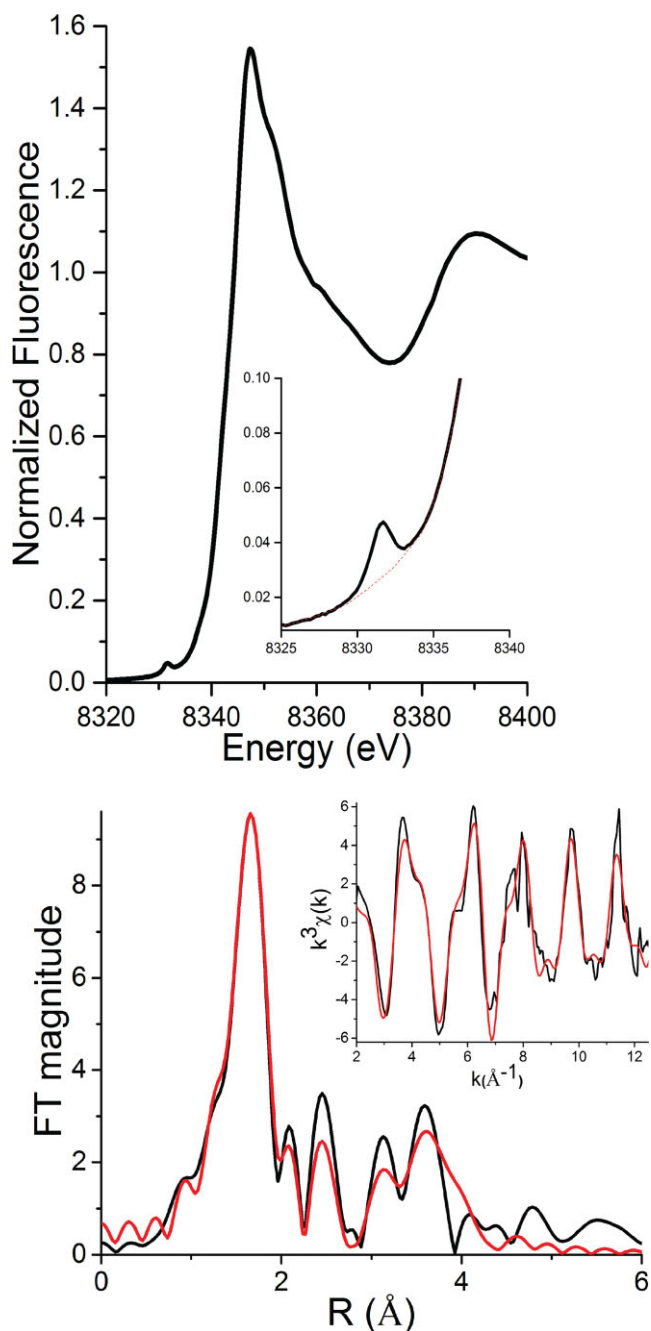


**Fig. 6.** Ni K-edge XAS of the Ni,Zn-HypA•UreE<sub>2</sub> complex at pH 7.2. Top: XANES spectrum Inset: Pre-edge feature associated with a 1s → 3d electronic transition (The baseline for area calculation is shown by the red dotted line.) Bottom: The Fourier-transformed (FT window = 2.0–12.5 Å<sup>-1</sup>) EXAFS spectrum (black line) and best fit from Table 2 (red line). Inset: Unfiltered k<sup>3</sup>-weighted EXAFS spectrum and calculated best fit model.

model featured three N/O scatterers at 2.04 Å and a single shell of three imidazole ligands with average Ni–N bond distance of 2.13 Å at an  $\alpha$ -angle 10°, and R = 4.9%.

Zn K-edge XAS was used to characterize the Zn(II)-site of HypA in the Ni,Zn-HypA•UreE<sub>2</sub> complex at pH 7.2 (Supplementary Fig. SI-10; Supplementary Table SI-3) and 6.3 (Supplementary Fig. SI-11; Supplementary Table SI-4). The EXAFS analysis on the Zn-site is consistent with four S-donor ligands with average Zn–S distances of 2.32(2) Å at both pH 7.2 and 6.3.

**Table 2.** Selected EXAFS fits for the Ni-site in the Ni,Zn-HypA•UreE<sub>2</sub> complex at pH 7.2<sup>a</sup>

Shell	r (Å)	$\sigma^2 (\times 10^{-3} \text{Å}^{-2})$	$\Delta E_0$	R-factor	Red. $\chi^2$
6 N/O	2.08 (1)	4 (0)	1 (2)	17.2	214.18
5 N/O	2.08 (1)	6(1)	0 (1)	10.2	144.00
1 Im0°	2.09 (1)	neg			
4 N/O	2.07 (1)	5 (2)	1 (1)	8.1	114.11
2 Im0°	2.09 (1)	2 (2)			
3 N/O	2.08 (1)	2 (1)	1 (1)	6.6	93.18
3 Im0°	2.09 (2)	6 (2)			
2 N/O	2.08 (1)	0 (1)	0 (1)	5.4	76.39
4 Im0°	2.08 (2)	8 (1)			
1 N/O	2.08 (1)	neg	0 (1)	5.3	76.04
5 Im0°	2.08 (1)	8 (1)			
3 N/O	2.06 (1)	2 (1)	0 (1)	6.5	91.57
3 Im5°	2.10 (2)	5 (2)			
3 N/O	2.04 (1)	4 (1)	0 (1)	5.3	74.76
3 Im10°	2.10 (1)	2 (0)			
<b>3 N/O</b>	<b>2.03 (1)</b>	<b>7 (2)</b>	<b>2 (1)</b>	<b>3.6</b>	<b>59.44</b>
<b>1 Im0°</b>	<b>2.07 (1)</b>	<b>1 (2)</b>			
<b>2 Im10°</b>	<b>2.09 (1)</b>	<b>1 (1)</b>			
2 N/O	2.03 (2)	3 (2)	0(1)	3.4	55.9
2 Im0°	2.09 (3)	7 (3)			
2 Im10°	2.09 (1)	0 (1)			

<sup>a</sup>The best fit is shown in bold.

neg = a negative value; parameters shown in red are unacceptable.

Errors indicated by numbers in parentheses represent uncertainties estimated by Artemis and are the changes in variables required to generate an increase in  $\chi^2$  of the value of reduced  $\chi^2$ .

## Protein and Ni(II) interactions by NMR spectroscopy

The 950 MHz <sup>1</sup>H, <sup>15</sup>N HSQC spectrum of apo,Zn-HypA (Fig. 7A), reporting the previously published assignment,<sup>62</sup> is not perturbed by the presence of 1 mM TCEP, so that all the following discussion refers to spectra obtained in its absence. In this spectrum, the signals of Met1 and His2 are not visible: the N-terminal NH<sub>3</sub><sup>+</sup> group of Met1 disappears because of fast exchange with the water signal, while the NH signal of His2 might undergo conformational exchange phenomena that broaden its line width beyond detection.

The spectrum of the apo,Zn-HypA•UreE<sub>2</sub> complex, containing <sup>15</sup>N-labeled HypA and unlabeled UreE<sub>2</sub> and pre-purified by SEC, is shown in Fig. 7B and reveals three main types of modifications as compared to the spectrum of isolated apo,Zn-HypA: some signals are not perturbed, some are only slightly shifted, and others are completely erased. Mapping the three types of signals on the NMR structure of apo,Zn-HypA<sup>62</sup> allowed us to conclude that the Zn-binding domain of HypA (residues 72–103), whose signals are not affected upon complex formation, is not involved in the interaction of HypA with UreE<sub>2</sub>, while essentially all of the Ni-binding domain (residues 1–68 and 107–117) features either a small recognizable shift or a large change in the H–N peak frequency. These perturbations are not localized on a distinct surface patch of the Ni-binding domain, but are generally spread throughout the domain, suggesting that significant structural perturbations are generated upon complex formation, which, even though likely involving a specific region, are allosterically transmitted to the whole domain.

Addition of one equivalent of Ni(II) to the preformed apo,Zn-HypA•UreE<sub>2</sub> complex (Fig. 7B) has the effect of making the amide NH signals of Ser9, Met39, and Glu103 as well as the side

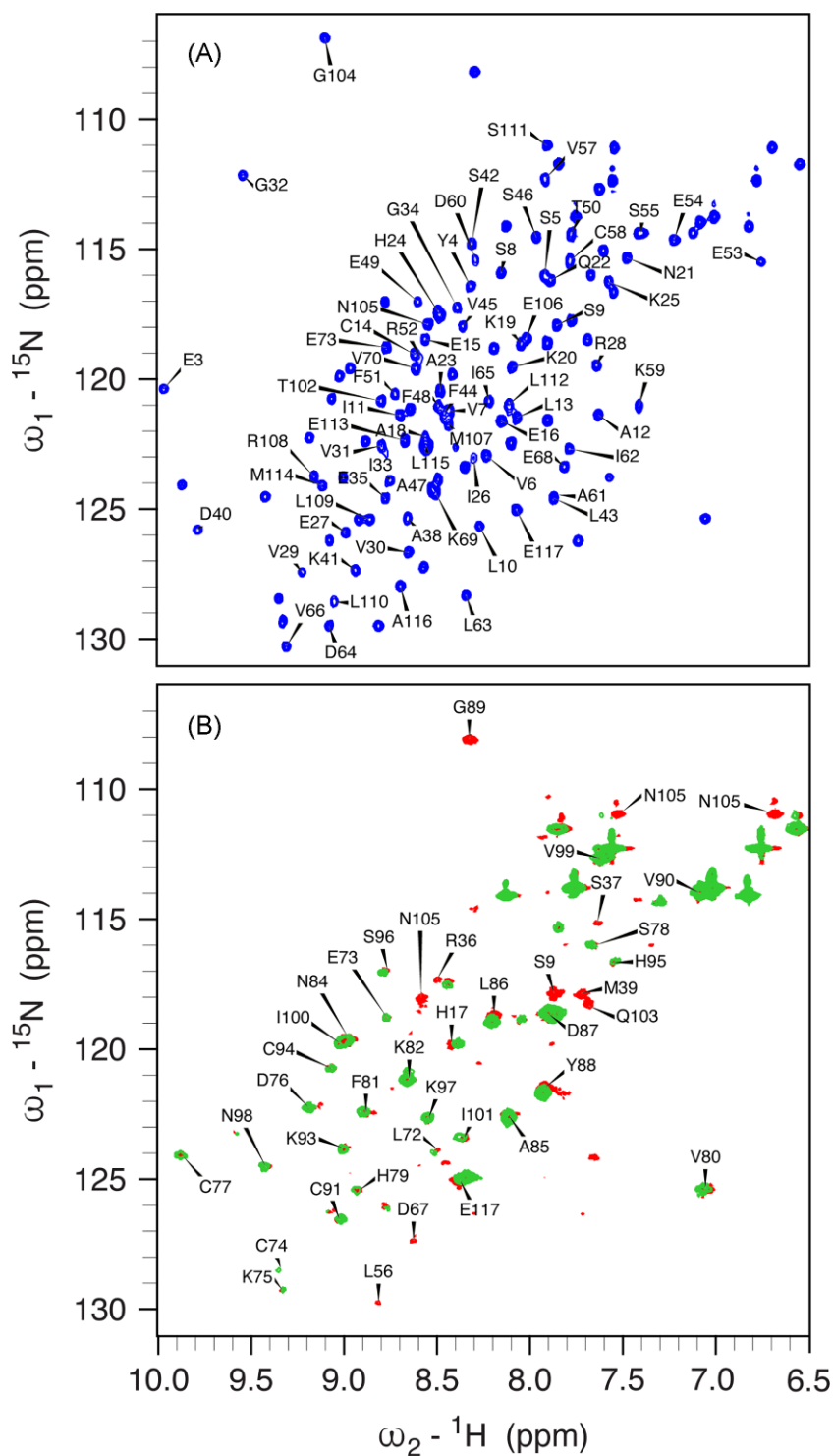


**Fig. 7.** 950 MHz  $^1\text{H}$ ,  $^{15}\text{N}$  HSQC spectra of apo,Zn-HypA (A, blue) and of the purified apo,Zn-HypA•UreE<sub>2</sub> complex (B, red). In panel A, the labels refer to the signals of residues of HypA that disappear in the spectrum of the complex with UreE<sub>2</sub>, while in panel B the labels indicate the residues of HypA that are unperturbed or only slightly shifted upon interaction with UreE<sub>2</sub>. In panel B, the spectrum of the Ni<sub>2</sub>Zn-HypA•UreE<sub>2</sub> complex is also shown in green.

chain -NH<sub>2</sub> signals of Asn105, disappear. These residues are located well within 10 Å of the N-terminal Ni-binding site on HypA, so that this effect can be attributed to the paramagnetism of the Ni(II) ion. The concomitant disappearance of Gly89, located on a loop in the Zn-binding domain and far from the Ni-binding site, could be caused by some undefined long distance allosteric mod-

ification, although mutation of Gly89 to Ala did not affect the delivery of Ni to urease, nor was it found to affect acidic viability in *Hp*.<sup>62</sup>

The interaction between Ni<sub>2</sub>Zn-HypA and UreE<sub>2</sub> was then investigated using  $^1\text{H}$  NMR spectra tailored for the observation of signals of residues bound to the Ni(II) center and affected by its

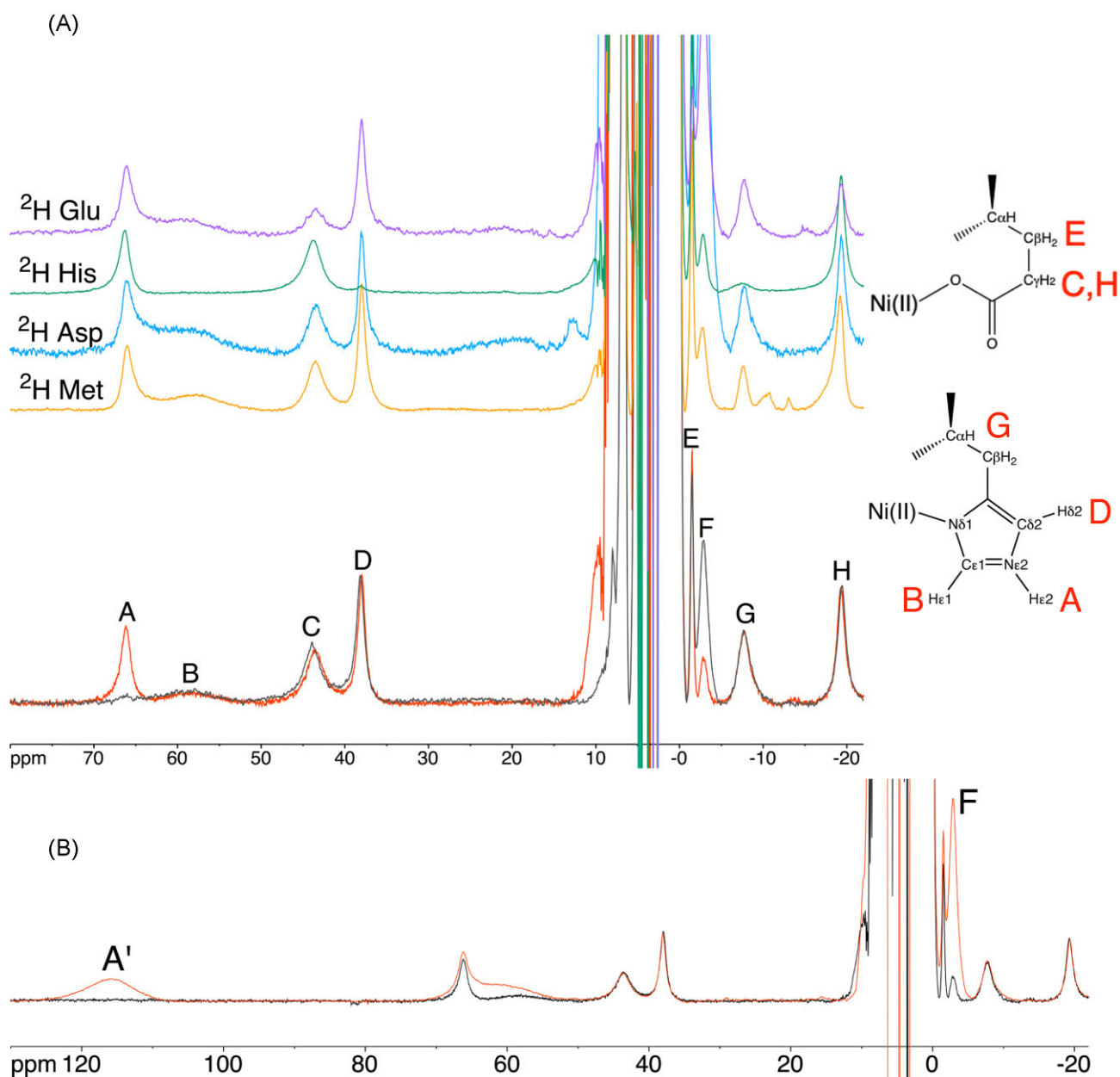


**Fig. 8.**  $^1\text{H}$  NMR spectra (400 MHz) of (A) Ni,Zn-HypA in  $\text{H}_2\text{O}$  (red) and  $\text{D}_2\text{O}$  (gray), together with the  $^1\text{H}$  NMR spectra of the corresponding selectively deuterated forms ( $^2\text{H}$  Met in orange,  $^2\text{H}$  Asp in blue,  $^2\text{H}$  His in green and  $^2\text{H}$  Glu in purple). The assignment of signals belonging to His2 is shown. Panel B shows the  $^1\text{H}$  NMR spectrum of Ni,Zn-HypA in the presence (red) and absence (black) of excess Ni.

paramagnetism. The spectrum of Ni,Zn-HypA (Fig. 8A) contains eight hyperfine-shifted signals (A–H) in the range from +80 to –20 ppm, arising primarily from contact and pseudo-contact shifts involving a single high spin ( $S = 1$ ) Ni(II) center coordinated to the N-terminal Met1 N atom, the amide N atoms of His2 and Glu3, and to an imidazole N atom of His2, with additional ligands filling the octahedral coordination environment of the metal ion coming from the side chain carboxylate of Glu3 and possibly a water molecule.<sup>23,62</sup> These signals have previously been tentatively assigned based on their chemical shift, linewidths, longitudinal relaxation times, temperature dependence, field dependence, solvent-exchange phenomena, and mono-dimensional NOE (Nuclear Overhauser Effect) experiments.<sup>62</sup>

In order to resolve some ambiguous assignments, we recorded the spectra of samples in which the putative Ni-binding amino

acids had been selectively deuterated. No change in the paramagnetic  $^1\text{H}$  NMR spectra of Ni,Zn-HypA containing deuterated methionine or aspartate residues could be observed (Fig. 8A), thus excluding Asp40 from the coordination sphere of Ni(II), in contrast to previous hypotheses,<sup>62,63</sup> as well as excluding any contribution of Met1 nuclei to the spectrum. On the other hand, the spectrum of HypA containing selectively deuterated histidines (Fig. 8A) shows that signals B, D, and G are essentially obliterated, indicating unequivocally that these signals belong to non-exchangeable protons of His2; concomitantly, the  $\text{D}_2\text{O}$ -exchangeable signal A is assigned to either H $\delta$ 1 or H $\epsilon$ 2 of the side chain imidazole of the Ni-bound His2. Considering the relatively larger linewidth of signal B as compared to that of signal D, and the fact that signal D features a significant NOE with signal A,<sup>62</sup> it can be concluded unambiguously that His2 must be bound to Ni(II) through its imidazole N $\delta$ 1

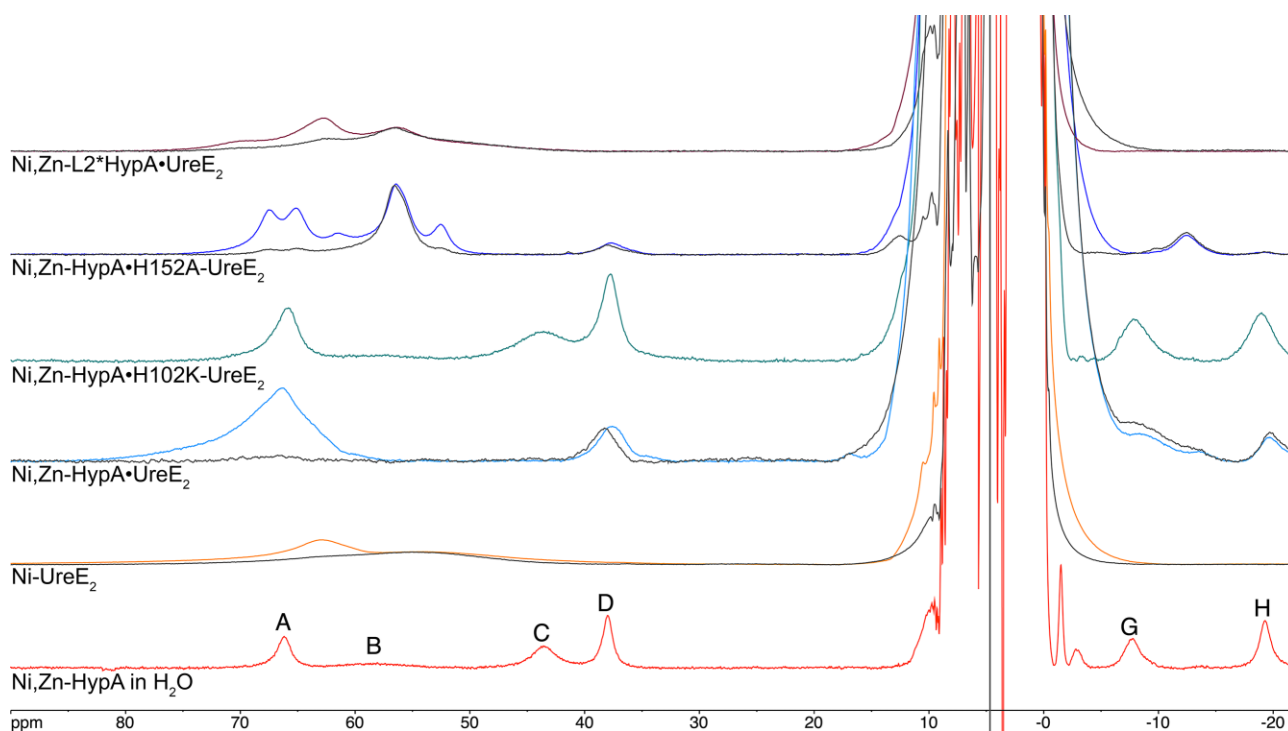


**Fig. 9.**  $^1\text{H}$  NMR spectra (400 MHz) of Ni,Zn-HypA in  $\text{H}_2\text{O}$  (red), Ni-UreE<sub>2</sub> (orange), Ni,Zn-HypA•UreE<sub>2</sub> (cyan), Ni,Zn-HypA•H102K-UreE<sub>2</sub> (green), Ni,Zn-HypA•H152A-UreE<sub>2</sub> (blue), and Ni,Zn-L2\*HypA•UreE<sub>2</sub> (brown). The corresponding spectra of the same proteins in  $\text{D}_2\text{O}$  are shown in dark gray.

atom (Fig. 8A). In this way, signal A is assigned to H $\epsilon$ 2, signal B to the ortho-like H $\epsilon$ 1, broadened by dipolar interactions because of its proximity to Ni(II), and signal D to the meta-like H $\delta$ 2, which experiences a smaller dipolar broadening because of its relatively larger distance from Ni(II). This assignment can be extended to signal G: the previously described lack of NOEs between signal G and any other signal assigned to His2<sup>62</sup> indicates that it belongs to either H $\alpha$  or a H $\beta$  of the side chain of His2.

The intensities of signals C, E, and H show a significantly decreased intensity in the NMR spectrum of HypA containing deuterated glutamate residues (Fig. 8A), indicating that they belong to the Ni-bound Glu3. This assignment is consistent with the observation of significant NOEs among signals C, E, and H in the NMR spectrum of WT Ni,Zn-HypA,<sup>62</sup> confirming that they belong to the same residue. The fact that they are not completely abolished is interpreted as an indication that the cell-free protocol used to produce this deuterated sample did not fully inhibit the transaminase activity, yielding only a partially, and not fully, deuterated sample as confirmed by mass spectrometry analysis (Supplementary Fig. SI-19). This is evidenced by the coexistence of several species, distributed broadly between two main peaks (13 242 and 13 268 Da) corresponding to partially deuterated samples (−35 and −9 Da as compared to the theoretical mass for the sample with fully deuterated glutamate residues, that is 13 277 Da), suggesting that there are multiple species partially deuterated. The relatively higher NOE intensities between signals C and H as compared to the NOEs involving signal E<sup>62</sup> suggests that signals C and H belong to the two H $\gamma$  geminal methylene proton pairs of the Glu3 side chain, while the much sharper and less shifted signal E can be safely assigned to a vicinal H $\beta$  of Glu3, respectively. The different linewidth of the signals of the two geminal protons could be explained by a conformation of the side chain of Glu3 that brings one of the two protons closer to

the Ni(II) center with respect to the other proton. These experiments showed also that signal F is not affected by deuteration of residues located in the coordination environment of Ni(II) in the Met-His-Glu (MHE) N-terminal motif of HypA. Considering that the intensity of signal F positively correlates with a broad signal A' found at 115.6 ppm, belonging to a non-exchangeable proton and observable only when an excess of Ni(II) is added to the protein (Fig. 8B), it can be concluded that signals A' and F are related to protons belonging to Cys14 and Cys58, found closely spaced in the Ni-binding domain. These residues are potentially able to bind an additional Ni(II) ion using their thiolate side chains. Indeed, H $\beta$  signals of Ni(II)-bound cysteines are typically broad and observed above 100 ppm<sup>64–66</sup> consistent with signal A', while the sharper and upfield-shifted signal F might be assigned to a cysteine H $\alpha$  proton.

The  $^1\text{H}$  NMR spectra of Ni,Zn-HypA, Ni-UreE<sub>2</sub>, the Ni,Zn-HypA•UreE<sub>2</sub> protein complex, and of the complexes formed between Ni,Zn-HypA and H102K-UreE<sub>2</sub> or H152A-UreE<sub>2</sub>, or between Ni-L2\*HypA and UreE<sub>2</sub> (Fig. 9) were essential to investigate the interaction of Ni,Zn-HypA with UreE<sub>2</sub>. In contrast to the well-defined hyperfine-shifted  $^1\text{H}$ -NMR spectrum observed for Ni,Zn-HypA (Fig. 9), the Ni-UreE<sub>2</sub> dimer reveals only a broad solvent-exchangeable envelope centered near 63 ppm and a very broad overlapping envelope of non-exchangeable resonances centered near 55 ppm (Fig. 9). These signals have been assigned to the exchangeable H-N $\delta$ 1 and non-exchangeable H $\delta$ 2 and H $\epsilon$ 1 resonances of the two Ni-bound His102A and His102B imidazole rings.<sup>67</sup> At variance with Ni,Zn-HypA, the absence of another relatively sharp non-exchangeable resonance is consistent with the coordination of Ni(II) by the imidazole N $\epsilon$  atom, in agreement with crystallography and XAS results.<sup>6</sup>

The spectrum of the Ni,Zn-HypA•UreE<sub>2</sub> WT protein complex (Fig. 9) exhibits a broad peak centered at ca. 67 ppm consisting of

exchangeable histidine imidazole H-N $\delta$ 1 or H-N $\epsilon$ 2, in addition to underlying non-exchangeable resonances (H $\delta$ 2 or H $\epsilon$ 1). The intensity of the exchangeable resonances indicates coordination of the Ni(II) center in the protein complex by several His imidazole side chains, and is consistent with the EXAFS analysis that estimates the presence of three-four imidazole ligands (*vide supra*).

In addition, two non-exchangeable resonances are observed at 38 and -19 ppm, which are absent in the spectrum of Ni-UreE<sub>2</sub> and correspond well to Ni,Zn-HypA signals D and H, assigned to His2 H $\delta$ 2 (signal D) and to a H $\gamma$  of Glu3 (signal H) in Ni,Zn-HypA. The concomitant absence of a signal corresponding to resonance C in Ni,Zn-HypA, assigned to the geminal H $\gamma$  partner of signal H, poses the question of the substantial larger broadening that affects signal C in the complex so that it is no longer visible, while signal H is slightly sharper than in the H102K-UreE<sub>2</sub> mutant complex above (from 970 to 900 Hz). This could be attributed to a modification of the metal-to-proton distances of the two Glu3 H $\gamma$  protons, which in turn could be caused by a variation of the Chi3 dihedral angle of the side chain of Glu3 (i.e. the dihedral angle Ni-C $\delta$ -C $\gamma$ -H $\gamma$ , see Discussion).

The hyperfine shifted <sup>1</sup>H-NMR spectrum of Ni,Zn-HypA•H102K-UreE<sub>2</sub> mutant (Fig. 9) is very similar to that obtained for the Ni,Zn-HypA protein, indicating that the coordination of the Ni(II) ion in HypA is not modified upon formation of the mutant complex, and that the presence of the pairs of His102A, B in the UreE<sub>2</sub> dimer is crucial for the formation of the Ni-binding site in the WT complex. The linewidths of the resonances observed in the Ni,Zn-HypA•H102K-UreE<sub>2</sub> complex are however significantly larger than in HypA alone (Fig. 9). The mere increase of the rotational correlation time of the larger protein complex (from 8 to 30 ns) is not sufficient to justify the ca. two-fold increase of the observed linewidths (see the quantitative treatment of the paramagnetic effects on relaxation in the Supplementary Information), while the data can be reasonably fitted by considering an electronic correlation time of  $8 \times 10^{-11}$  s, slightly larger than that in Ni,Zn-HypA complex ( $5 \times 10^{-11}$  s). Such an increase of the electronic relaxation rate could be explained with a slight change in the coordination geometry of Ni(II) without significantly affecting the chemical shifts because the hyperfine constants are not modified.

The hyperfine-shifted <sup>1</sup>H-NMR spectrum obtained for the Ni,Zn-HypA•H152A-UreE<sub>2</sub> complex does not closely resemble the spectra obtained from either the HypA or UreE<sub>2</sub> Ni(II) complexes (Fig. 9). At least four solvent exchangeable imidazole HN resonances are observed for a protein complex that has only three of the original imidazole residues (a pair of His102 residues from UreE<sub>2</sub> and the His2 residue from HypA). Based on the species distribution obtained by the analysis of the ITC data (Fig. 4C), we suggest that these signals might arise from a mixture of Ni,Zn-HypA•H152A-UreE<sub>2</sub>, Ni-H152A-UreE<sub>2</sub> and Ni-H152A-UreE<sub>4</sub>, possibly coordinated to a mixture of N $\epsilon$  and N $\delta$  imidazole atoms, with some residual Ni,Zn-HypA.

The insertion variant L2\*HypA was also used to form a complex with UreE<sub>2</sub> and examined by NMR (Fig. 9). The fact that L2\*HypA forms a Ni,Zn-L2\*HypA•UreE<sub>2</sub> protein complex is confirmed by SEC-MALS, and that the protein complex binds Ni(II) is established by ITC (Table 1 and in Hu *et al.*<sup>25</sup>). However, the hyperfine spectrum obtained for this complex contains none of the non-exchangeable proton resonances associated with HypA, and the remaining broad resonances resemble those of the Ni(II) complex of UreE<sub>2</sub>. This result indicates that Ni(II) is bound solely to UreE<sub>2</sub> in the complex formed between L2\*HypA, and is consistent with

the large decrease in Ni(II) binding affinity in the L2\*HypA variant (*vide supra*).

## Computation of the structural model of the Ni,Zn-HypA•UreE<sub>2</sub> complex

Based on all the available experimental evidence, a viable structural model of the Ni,Zn-HypA•UreE<sub>2</sub> protein complex was calculated. The structural modelling procedure consisted of two steps: an initial model of the apo,Zn-HypA•UreE<sub>2</sub> protein complex was generated by using a procedure that takes advantage of two state-of-the-art approaches, namely AlphaFold2<sup>40</sup> and RoseTTAFold<sup>41</sup>; these algorithms yielded excellent results in the most recent CASP14 experiment<sup>68</sup> and were also applied to model proteins involved in the import/export of Ni(II) ions through cellular membranes.<sup>69</sup> Subsequently, a model of the Ni-binding site located at the interface between HypA and UreE<sub>2</sub> was constructed through a data-driven procedure already used in the case of other metalloproteins involved in the activation of urease<sup>43</sup> or nickel binding transcriptional regulators.<sup>44,45</sup>

The best model structure of the apo,Zn-HypA•UreE<sub>2</sub> complex is reported in Fig. 10A (see Supplementary Figs. SI-12–15 for more details on the generated models). Both HypA and UreE<sub>2</sub> are well-modelled and show structures nearly identical to the available experimental NMR and X-ray crystal structures, respectively (see Supplementary Fig. SI-16 for a comparison). The main differences are the presence, in the UreE<sub>2</sub> model, of the C-terminal regions that were not observed in the crystal structure because of disorder in the solid state, and a slightly different orientation of the HypA Zn-binding domain caused by the flexible unstructured linker region between the Zn- and the Ni-binding domains. In this model, HypA interacts with the UreE<sub>2</sub> dimer in two regions: (i) the N-terminal  $\alpha$ -helix that is in close contact with the Ni(II) binding region of UreE<sub>2</sub>, specifically with the His102A and His102B from both UreE monomers, and (ii) the  $\beta$ -sheet located in the Ni-binding domain, which is found to interact with one of the C-terminal tails of UreE<sub>2</sub> and results in an extended  $\beta$ -sheet. Such an extended intermolecular  $\beta$ -sheet is also present in all the other apo,Zn-HypA•UreE<sub>2</sub> model structures (see Supplementary Figs. SI-12–15), even though the involved UreE<sub>2</sub> C-terminus is different in each model (in one case, both C-terminals of UreE<sub>2</sub> are engaged in the interaction with HypA). This result suggests an unanticipated role for the UreE<sub>2</sub> C-terminal regions in stabilizing the protein–protein complex. In agreement with the <sup>1</sup>H,<sup>15</sup>N HSQC NMR spectrum discussed earlier (Fig. 7), the HypA Zn-domain does not appear to be involved in the formation of the complex with the UreE<sub>2</sub> dimer. Interestingly, the calculation of the model structure of the apo,Zn-HypA•UreE<sub>2</sub> complex without including the C-terminal regions of UreE<sub>2</sub> (residues 152–170) results in a completely different structure that is inconsistent with the experimental NMR observations. This model features larger portions of HypA, including the Zn-domain, involved in the protein–protein interaction, and the N-terminal region of HypA no longer poised to build a Ni(II)-binding site in correspondence to the His102A and His102B residues on UreE<sub>2</sub> (Supplementary Fig. SI-17), highlighting the importance of the elongated C-termini.

In the modelling of the Ni-binding site in the Ni,Zn-HypA•UreE<sub>2</sub> complex, the metal ion was restrained to binding the N $\epsilon$  atoms of His102A and His102B from both UreE<sub>2</sub> monomers, in agreement with the crystal structure of the Ni-bound UreE<sub>2</sub><sup>6</sup>, in addition to the backbone N atoms of His2 and Glu3, the imidazole N $\delta$  of His2 and the carboxylate O $\epsilon$ 1 atom of Glu3 on the HypA side, with distances taken from the XAS data analysis (Table 3), while no restraints were added to constrain a specific coordina-

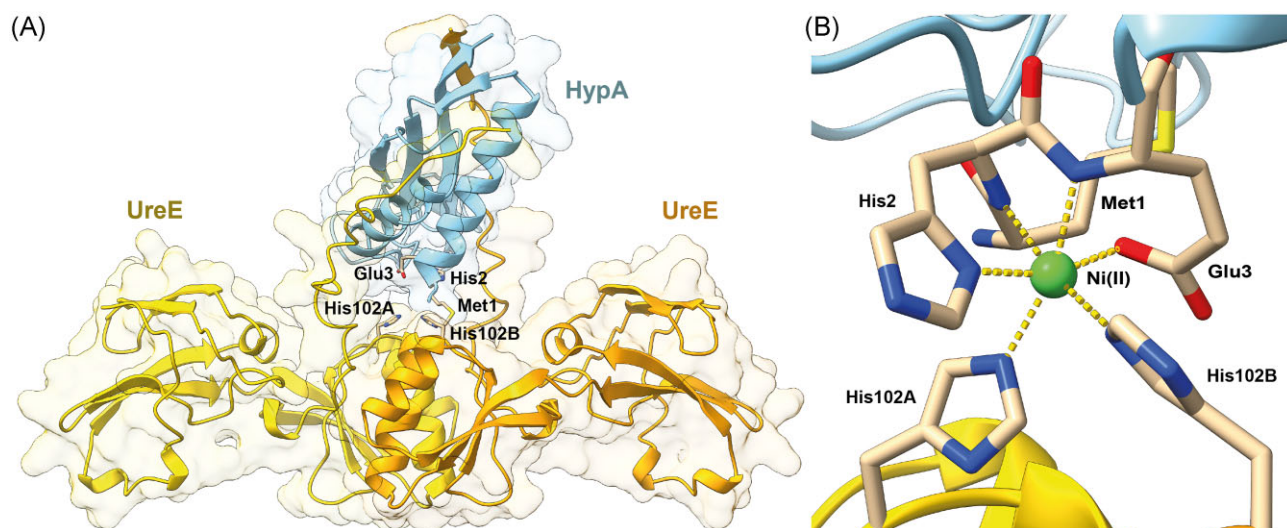


**Fig. 10.** (A) Ribbon diagram and molecular surface of the apo,Zn-HypA•UreE<sub>2</sub> complex model structure. HypA is in light blue, while UreE<sub>2</sub> monomers are in yellow and orange. Residues involved in Ni(II) binding are in sticks, colored according to the atom type. (B) Data-based model of the Ni(II)-binding site located at the interface between HypA and UreE<sub>2</sub>. The Ni(II) ion is shown as a green sphere, while the coordination bonds are indicated with yellow dashed lines.

**Table 3.** Distances, angles, and dihedral constraints used in the modelling of Ni-HypA•UreE<sub>2</sub>. All constraints in the form mean  $\pm$  1 standard deviation

Constrained atoms		Distance (Å)	
Ni(II)-His2(HypA,N)		2.00 $\pm$ 0.05	
Ni(II)-His2(HypA, N $\delta$ )		2.10 $\pm$ 0.05	
Ni(II)-Glu3(HypA,N)		2.00 $\pm$ 0.05	
Ni(II)-Glu3(HypA,O $\epsilon$ 1)		2.00 $\pm$ 0.05	
Ni(II)-His102(UreE,Ne)		2.10 $\pm$ 0.05	
Bonded atoms		Constrained atoms	Angle (degrees)
Ni(II)-His2(HypA,N)		Ni(II)-His2(N)-Met1(C)	120 $\pm$ 10
		Ni(II)-His2(N)-His2(C $\alpha$ )	120 $\pm$ 10
Ni(II)-His2(HypA, N $\delta$ )		Ni(II)-His2(N $\delta$ )-His2(C $\gamma$ )	120 $\pm$ 10
		Ni(II)-His2(N $\delta$ )-His2(C $\epsilon$ )	120 $\pm$ 10
Ni(II)-Glu3(HypA,N)		Ni(II)-Glu3(N)-His2(C)	120 $\pm$ 10
		Ni(II)-Glu3(N)-Glu3(C $\alpha$ )	120 $\pm$ 10
Ni(II)-Glu3(HypA,O $\epsilon$ 1)		Ni(II)-Glu3(O $\epsilon$ 1)-Glu3(C $\delta$ )	109 $\pm$ 5
Ni(II)-His102(UreE,Ne)		Ni(II)-His(N $\epsilon$ )-His(C $\delta$ )	120 $\pm$ 10
		Ni(II)-His(N $\epsilon$ )-His(C $\epsilon$ )	120 $\pm$ 10
Bonded atoms		Constrained atoms	Dihedral (degrees)
Ni(II)-His2(HypA,N)		Ni(II)-His2(N)-Met1(C)-Met1(O)	180 $\pm$ 10
Ni(II)-His2(HypA, N $\delta$ )		Ni(II)-His(N $\delta$ )-His(C $\epsilon$ )-His(N $\epsilon$ )	180 $\pm$ 10
		Ni(II)-His(N $\delta$ )-His(C $\gamma$ )-His(C $\delta$ )	180 $\pm$ 10
Ni(II)-Glu3(HypA,N)		Ni(II)-Glu3(N)-His2(C)-His2(O)	180 $\pm$ 10
Ni(II)-His102(UreE,Ne)		Ni(II)-His(N $\epsilon$ )-His(C $\epsilon$ )-His(N $\delta$ )	180 $\pm$ 10
		Ni(II)-His(N $\epsilon$ )-His(C $\delta$ )-His(C $\gamma$ )	180 $\pm$ 10

tion geometry around the metal ion. In Fig. 10B the result of the metal site modelling procedure is shown: the Ni(II) is coordinated to the six ligands, spontaneously assuming a slightly distorted octahedral coordination geometry (root mean square deviation with respect to an ideal coordination geometry = 0.336 Å). The Ni(II) ion is bound to the HypA His2 imidazole ring N $\delta$  atom, and to the N $\epsilon$  atoms of the imidazoles of the UreE<sub>2</sub> His102 residues, consistent with the hyperfine-shifted NMR results (*vide supra*). The remaining ligands are provided by the His2 and Glu3 amide N-donors, and the Glu3 sidechain carboxylate. The Ni-bound His imidazole ligands are in a *fac* configuration with the His2 imidazole ring *trans* to the side chain of HypA Glu3, which in turn is *cis* with respect to the amide N atoms of HypA His2 and Glu3. The analysis of the structure did not reveal any distortion from the

ideal geometries for the residues involved in the metal binding. With respect to the model structure of the apo,Zn-HypA•UreE<sub>2</sub> complex previously calculated, a slight unfolding of the HypA N-terminal helix is observed, possibly to allow the formation of the Ni(II)-binding site. Indeed, the flexibility of the N-terminal helix had already been described by atomistic molecular dynamics calculations carried out on apo,Zn-HypA.<sup>62</sup>

An alternative model of the Ni(II)-binding site in the Ni,Zn-HypA•UreE<sub>2</sub> complex, generated by including the N-terminal nitrogen atom from HypA Met1 as a nickel ligand and excluding the backbone N atoms from HypA Glu3, resulted in steric clashes involving several atoms of Glu3 (see Supplementary Fig. SI-18 in the Supplementary Information). The latter clashes can be removed only through the denaturation of the initial ten HypA residues, a result that is not supported by experimental evidence or molecular dynamics simulations.<sup>62</sup>

### Computation of the Ni-site in the Ni,Zn-HypA•UreE<sub>2</sub> complex and in Ni,Zn-HypA

On the basis of the previously achieved model of the Ni, Zn-HypA•UreE<sub>2</sub> complex, derived on the basis of restrained molecular mechanics calculations, a computational model of the Ni-site was derived and geometry optimized by using DFT computations. The geometry of the optimized model (Fig. 11A) does not change significantly from the more approximate model obtained through homology modelling, confirming the reliability of the present prediction. The Ni(II) coordination geometry is octahedral with only small distortions (RMSD from an ideal octahedral geometry = 0.150 Å).

From this model of the Ni-site in the Ni,Zn-HypA•UreE<sub>2</sub> complex, two tentative model structures of the nickel-binding site of HypA were generated. In the first model, the two histidine residues from the UreE dimer were removed and the conformation of HypA Met1 was changed manually in order to bring the N-terminal nitrogen in the vicinity of the Ni(II) ion. The optimized structure of such a model (Fig. 11B) resulted in a quite distorted octahedral Ni(II) coordination geometry (RMSD = 0.341 Å) where the Glu3 carboxylate is bound in a bidentate fashion to the Ni(II) ion.



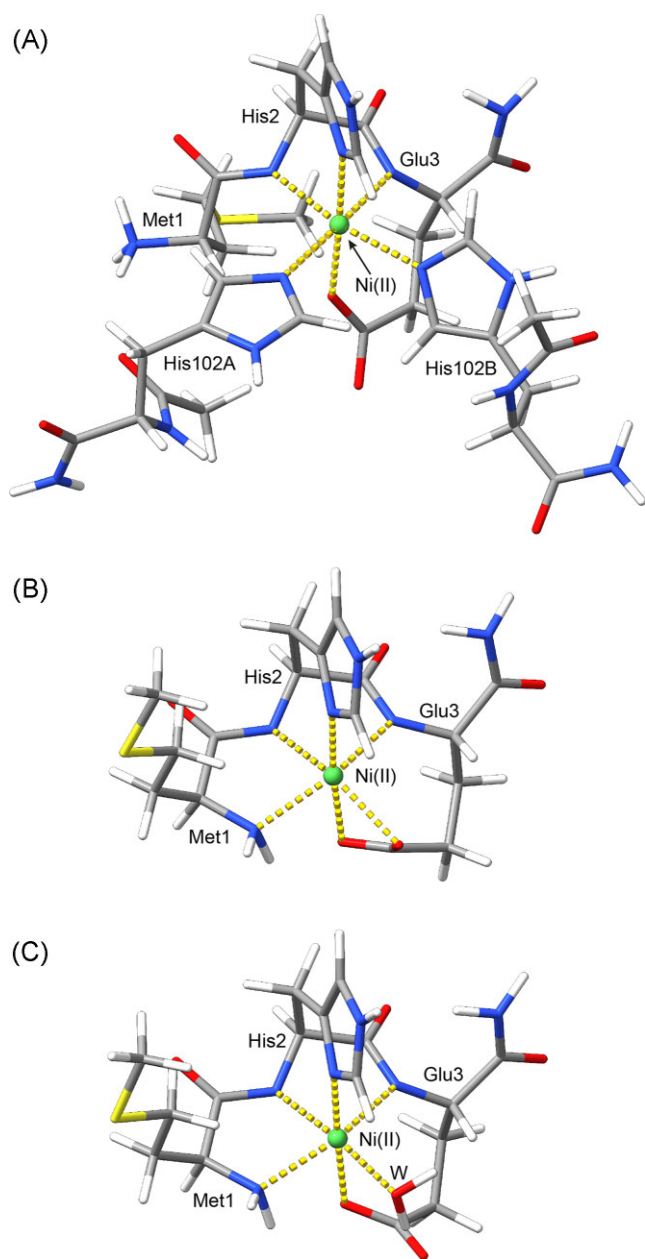


**Fig. 11.** B3LYP/G 6–31(p, d) with diffuse functions on all atoms optimized geometries of the Ni-site in the Ni,Zn-HypA•UreE<sub>2</sub> complex (A) and in Ni,Zn-HypA (B and C). Atoms are colored according to atom type and coordination bonds are reported using dashed yellow lines.

Finally, we considered an alternative model for the Ni(II) site in HypA, which included the presence of a water molecule as Ni(II) ion sixth ligand. The result of the geometry optimization of this HypA Ni-site model are reported in Fig. 11C. In this model, the Ni(II) coordination geometry is less distorted than in the model involving a bidentate Glu3 carboxylate group (RMSD = 0.196 Å).

These models were then used to explain some features of the paramagnetically shifted NMR signals. The spectrum of Ni-HypA (Figs. 8 and 9) features signals C and H, assigned to a geminal Hy pair of Glu3, displaying different linewidths, suggesting two different nickel-proton distances. In the DFT-optimized model of holo-HypA containing a bidentate mode for Ni(II) coordination by Glu3 these distances are 4.2 and 4.4 Å, while in the model featuring a bound solvent molecule, the distances are 4.6 and 4.7 Å. A quantitative analysis of the paramagnetic transverse relaxation (see

Supplementary Information and Supplementary Fig. SI-21) suggests that a slight variation of the Chi3 dihedral angle for Glu3 with respect to the model calculated *in vacuo* is sufficient to bring the  $\gamma$ CH<sub>2</sub> protons at distances from Ni(II) compatible with the observed linewidths. Similarly, the linewidths of signals C and H in the Ni,Zn-HypA-(H102K)UreE<sub>2</sub> mutant complex (Fig. 9), in which Ni(II) is retained by HypA because of the mutation of the nickel-binding residues on UreE<sub>2</sub>, a similar treatment suggests again that a minor rotation of Chi3, together with an minor increase of the electronic relaxation time, allows the reproduction of the experimental linewidths. Finally, in the NMR spectrum of Ni,Zn-HypA-UreE<sub>2</sub> (Fig. 9), signal C disappears while signal H is still visible and actually decreases its linewidth. Assuming 3 kHz as a threshold limit for signal detection, using the same quantitative treatment of the nuclear relaxation as mentioned earlier, these observations support a rotation of the Chi3 angle by ca. 40° with respect to the model calculated *in vacuo*. In all these cases, the difference of this geometric parameter between the theoretical model and the experimental data can be justified by the presence of the protein scaffold surrounding the Ni(II)-binding site.

## Discussion

A unique feature of nickel trafficking in *Hp* is the use of the metallochaperone HypA to mediate Ni incorporation in two distinct enzymes, urease and hydrogenase.<sup>10,11</sup> In general, metallochaperones are able to transfer the specific metals required for enzyme active sites via formation of specific protein–protein complexes.<sup>4</sup> In the case of [Ni,Fe]-hydrogenase, a complex formed between HypA and the apo-large subunit of the hydrogenase heterodimer appears to be involved in Ni incorporation<sup>3</sup>. For urease, the analogous transfer is mediated by UreE<sub>2</sub>.<sup>8,70</sup> The requirement of a second metallochaperone in the delivery of Ni to urease suggests the involvement of additional protein complexes, as well as perhaps implying a higher degree of control over the process. Indeed, an interaction between HypA and UreE<sub>2</sub> has been shown to be required for maturation of urease<sup>12</sup> and a protein–protein complex was previously described as consisting of one HypA molecule and one UreE<sub>2</sub> dimer.<sup>25</sup> This complex was found to bind Ni(II) many orders of magnitude tighter than either the HypA or UreE<sub>2</sub> proteins, implying the existence of a unique Ni(II)-binding site formed in the protein complex.<sup>25</sup> The focus of this work is to more fully characterize and elaborate the structure of the HypA•UreE<sub>2</sub> complex and the novel high-affinity Ni(II) site in the protein complex and elucidate mechanistic details of Ni binding.

The protein–protein interactions and the Ni-binding affinities of the complexes formed between WT- and L2\*-HypA proteins and UreE<sub>2</sub> protein and His102/152 UreE<sub>2</sub> variants were assessed by a combination of SEC–MALS and ITC experiments that were interpreted using a global fitting model that takes into account five equilibria (Eqn. 4). This method allowed each equilibrium involved in processes of forming Ni,Zn-HypA•UreE<sub>2</sub> to be examined and the effects of protein modifications on individual equilibria to be assessed. The results shown in Table 1 allow several observations to be made:

- (i) The SEC–MALS data show that the protein complexes form regardless of mutations in the Ni(II)-binding site (Fig. 1), although the affinity of the proteins (Table 1) is weakened in the Ni site variants (e.g. apo, Zn-L2\*HypA•UreE<sub>2</sub> ( $K_D = 1.7 \mu\text{M}$ ) vs. apo,Zn-HypA•UreE<sub>2</sub> ( $K_D = 0.8 \mu\text{M}$ )). Therefore, the Ni ligands are not critical for protein complex formation.

- (ii) Apo, Zn-HypA•UreE<sub>2</sub> contains a novel high-affinity Ni-binding site with a K<sub>D</sub> of about 0.15 nM that is not present in either component protein. The sub-nanomole K<sub>D</sub> indicates that the apo,Zn-HypA•UreE<sub>2</sub> protein complex binds Ni much tighter than either of the component proteins (K<sub>D</sub> = 0.9 and 0.3 mM for HypA and UreE<sub>2</sub>, respectively). The values of K<sub>D</sub> obtained for HypA and UreE<sub>2</sub> are characteristic of metallochaperones in general, which typically feature values of K<sub>D</sub> in the μM range.<sup>26</sup> The sub-nanomole value K<sub>D</sub> observed for Ni,Zn-HypA•UreE<sub>2</sub> is more characteristic of Ni-responsive transcriptional regulators, such as InrS (K<sub>D</sub> ~ 10<sup>-10</sup> M)<sup>27</sup> and suggests a different function for the protein complex.
- (iii) Mutations involving metal-binding ligands in the component proteins (the HypA N-terminal amine in L2\*, His102 and His152 in UreE<sub>2</sub>) significantly weaken the Ni affinity of the novel Ni-binding site in the protein complex (Table 1). This result shows that ligands from both component proteins are involved in forming the high-affinity binding site in apo,Zn-HypA•UreE<sub>2</sub> and indicates that the high-affinity site forms at a protein–protein interface.

The robust formation of the Ni,Zn-HypA•UreE<sub>2</sub> allowed for isolation and characterization of Ni,Zn-HypA•UreE<sub>2</sub>. HypA is a small, elongated protein that contains an intrinsic Zn-binding site associated with two CXXC sequences near the C-terminus and a Ni-binding site located at the N-terminus.<sup>62</sup> The Zn-binding domain is composed of a β-structure and is connected to the larger Ni-binding domain by a flexible linker.<sup>62</sup> The Ni-binding domain is composed of two α-helices and a three-stranded parallel/antiparallel β-sheet.<sup>62</sup> <sup>1</sup>H,<sup>15</sup>N HSQC spectra at 950 MHz of labeled HypA protein in the apo,Zn-HypA•UreE<sub>2</sub> complex (Fig. 7) show that the Zn binding domain is not involved in forming the protein complex. In contrast, many perturbations are found in the Ni-binding domain. This result is consistent with analogous experiments carried out using a form of HypA mutated at the N-terminus and containing a Gly-Ser extension,<sup>59</sup> demonstrating that the protein–protein interaction does not depend greatly on the N-terminus of the HypA polypeptide. This observation is also consistent with the studies of the L2\*-HypA variant (involving an insertion of Leu between Met1 and His2) that greatly weakens Ni(II) binding to HypA (by a factor of > 700, Table 1) and the HypA•UreE<sub>2</sub> complex (by a factor of ~400),<sup>23</sup> but affects the protein–protein interaction to a much smaller extent (Table 1 and reference<sup>25</sup>). A potential explanation for the global structural changes in the Ni-binding domain of HypA in apo,Zn-HypA•UreE<sub>2</sub> observed by NMR, as well as for the insensitivity of the protein–protein interaction to the HypA N-terminal sequence, was obtained from computational modelling of the apo,Zn-HypA•UreE<sub>2</sub> complex with AlphaFold2<sup>40</sup> and RoseTTAFold.<sup>41</sup> The resulting models show that the N-terminal Ni-binding site of HypA contacts the dimer interface of UreE<sub>2</sub> near to the known Ni-binding ligands—a pair of His102 residues—and that the rest of the protein is locked in the embrace of the UreE<sub>2</sub> C-terminal sequence, which forms additional strands of β-sheet with the HypA Ni-binding domain three-stranded β-sheet (Fig. 10A).

Structural characterizations of the metal sites were performed on the isolated Ni,Zn-HypA•UreE<sub>2</sub> protein complex by XAS. These studies revealed that the Zn site in Ni,Zn-HypA•UreE<sub>2</sub> is a Zn(SCys)<sub>4</sub> site that is unperturbed from that found in HypA protein alone,<sup>62</sup> in agreement with the NMR results and computational models that show that the Zn-binding domain is not involved in the formation of the complex (*vide supra*). The interfacial

Ni site in Ni,Zn-HypA•UreE<sub>2</sub> was shown to be a six-coordinate distorted octahedral site composed of three or four His imidazole ligands and totaling six O, N-donor ligands (Table 2 and Fig. 6). Given the odd number of His ligands available in the metal-binding sites of the two component proteins, the data are most consistent with three His imidazole ligands, His2 from HypA and a pair of His imidazole ligands from the UreE<sub>2</sub> dimer that are assigned to a pair of His102 ligands on the basis of the ITC and NMR results (*vide infra*).

Further structural details regarding the Ni site in Ni,Zn-HypA•UreE<sub>2</sub> were obtained by NMR. The HypA protein exhibits eight hyperfine-shifted signals (A–H) in the range from +80 to –20 ppm (Fig. 8). These signals had previously been assigned to amino acid residues based on their chemical shift, linewidths, longitudinal relaxation times, temperature dependence, field dependence, solvent-exchange phenomena and NOEs, that left some assignments ambiguous, particularly those that might be due to Met1, Glu3, or Asp40 α- or methylene-protons.<sup>62</sup> The spectrum of Ni,Zn-HypA was re-examined using HypA samples that contained selectively deuterated amino acids. This confirmed the assignments of signals A, B, D and G to His2 protons, and allowed the unambiguous assignment of signals C, E, and H to Glu3 (Fig. 8A). No signals were found to be associated with Met1 or with Asp40. This is not surprising for Met1 bound by the N-terminal amine,<sup>23</sup> considering that the paramagnetism of the bound Ni(II) is expected to obliterate the signals of both the terminal amine protons as well as the Hα proton of Met1, broadened beyond detection because of decreased relaxation time; moreover, this also indicates that Asp40 is not a ligand for Ni(II). The consideration of Asp40 as a ligand derives from its inclusion as a carboxylate O-donor in the Ni site based on NMR studies of a HypA complex modified with an N-terminal Gly-Ser extension.<sup>63</sup> This extension of the N-terminus in HypA induces the formation of an artefactual planar and diamagnetic Ni(II) site, instead of a now well-established pseudo-octahedral metal-binding site in the WT protein, which causes the Ni(II) ion to be paramagnetic.<sup>23,62</sup> Thus, the involvement of Asp40, while consistent with the disappearance of NMR signals near Asp40,<sup>62</sup> is likely an artifact of the structural alteration of the Ni site in the N-terminally modified HypA protein. The combination of XAS structural information and this NMR data lead to a structure for the Ni complex in HypA that involves ligation by the N-terminal amine of Met1, the imidazole Nδ and amide N of His2, the side-chain carboxylate and amide N of Glu3, and one O/N-donor lacking any hyperfine-shifted <sup>1</sup>H-NMR resonances that is consistent with a water-derived ligand or the presence of a bidentate Glu3 carboxylate.

The hyperfine-shifted <sup>1</sup>H-NMR of the Ni,Zn-HypA•UreE<sub>2</sub> complex (Fig. 9) reveals several resonances that are analogous to those assigned to His imidazole ligands in HypA and UreE<sub>2</sub>, including signal D. The observation of signal D confirms that the HypA His2 ligand is present in the high-affinity Ni-binding site of the complex and that its coordination mode is unaltered from the HypA site. The increase in the intensity of the envelope of resonances corresponding to solvent-exchangeable protons assigned to N-H protons of His imidazole ligands relative to signal D is consistent with the presence of three His imidazole ligands found in the EXAFS analysis (*vide supra*). The identity of the two additional His imidazole ligands in Ni,Zn-HypA•UreE<sub>2</sub> was confirmed by the hyperfine-shifted NMR spectrum of the Ni,Zn-HypA•H102K-UreE<sub>2</sub> variant, which exhibits resonances only from HypA ligands.

Notably absent from the spectrum of HypA•H102K-UreE<sub>2</sub> is signal C, assigned to a methylene proton in the Glu3 side chain. At first glance, the absence of signal C might suggest that the

Glu3 carboxylate has been lost as a Ni ligand in the protein complex. This would be consistent with the substitution of this ligand and the putative water-derived ligand by the pair of UreE<sub>2</sub> His102 residues and the retention of all other HypA ligands, including the N-terminal amine, which cannot be detected by NMR nor unambiguously assigned by EXAFS analysis. However, signal H is still present in the hyperfine-shifted NMR spectrum of Ni,Zn-HypA•UreE<sub>2</sub> and has been assigned to a methylene proton on Glu3 that is geminal to the proton giving rise to signal C on the basis of an NOE measurement.<sup>62</sup> This fact argues for retention of the Glu3 carboxylate in the HypA•UreE<sub>2</sub> complex. The disappearance of signal C can be explained as arising from a reorientation of the methylene protons (as might accompany a bidentate to monodentate conversion) such that the proton giving rise to signal C is much closer to the Ni center in the HypA•UreE<sub>2</sub> complex than in HypA, leading to dipolar line broadening to the extent that it is no longer detected.

The inclusion of the Glu3 carboxylate in the Ni,Zn-HypA•UreE<sub>2</sub> complex requires that some other ligand is lost in addition to substitution of water (or change in carboxylate coordination). This ligand must lack any observable hyperfine-shifted <sup>1</sup>H-NMR signal. Based on the structure of the Ni(II) site in the HypA protein, three possibilities exist: the Met1 amine, the His2 amide N atom, or the Glu3 amide N-atom. The lack of perturbation of any resonances associated with His2 in Ni,Zn-HypA•UreE<sub>2</sub> relative to the HypA complex argues for retention of the His2 amide N-donor, which enforces the N $\delta$  coordination of the His2 imidazole. The fact that Ni-binding affinities are greatly reduced and the structures of the Ni sites are altered in both the L2\*-HypA complex and in Ni, Zn-L2\*-HypA•UreE<sub>2</sub> argues for retention of the Met1 amine in Ni,Zn-HypA•UreE<sub>2</sub>. In the case of HypA, the L2\* insertion decreases Ni binding affinity (Table 1), prevents nickelation of urease *in vivo*, and causes the structure to become five-coordinate and adopt a low-spin (diamagnetic) electronic configuration.<sup>23</sup> In Ni, Zn-L2\*-HypA•UreE<sub>2</sub>, the affinity of the Ni site is also decreased, and the hyperfine-shifted NMR resembles that of Ni-UreE<sub>2</sub>, consistent with the loss of coordination of HypA ligands and the complete transfer of Ni(II) from HypA to UreE<sub>2</sub> in the protein complex. However, inclusion of the N-terminal amine in Ni,Zn-HypA•UreE<sub>2</sub> and dissociation of the Glu3 amide N atom is not compatible with the modelling results, given the attendant constraints (*vide supra*), which support only the dissociation of the N-terminal amine in Ni,Zn-HypA•UreE<sub>2</sub>.

The details of how of Ni,Zn-HypA•UreE<sub>2</sub> functions in the maturation of *Hp* urease remain incomplete. In other organisms, the presence of UreE<sub>2</sub> is sufficient to provide Ni(II) to the urease maturation pathway by delivering Ni to UreG (a soluble GTPase involved in the urease maturation process) via the heterodimeric Ure(GE)<sub>2</sub>, forming a UreG dimer with an interfacial Ni(II) site.<sup>5,8,71</sup> Ni-UreG<sub>2</sub> then completes nickelation of apo-urease via a ternary Ure(DFG)<sub>2</sub> protein complex.<sup>72,73</sup> In *Hp*, while UreE<sub>2</sub> is a requirement for urease maturation, the process also requires HypA under physiological conditions.<sup>4</sup> NMR-based results show that no complex is formed between Ni,Zn-HypA•UreE<sub>2</sub> and UreG (Supplementary Fig. SI-20), suggesting that UreE<sub>2</sub> can interact with either HypA or UreG, but not both simultaneously, presumably because both complexes involve the same UreE<sub>2</sub> interface that comprises the conserved His102A, B on the homodimer surface. HypA is known to acquire Ni(II) from HypB, which in turn acquires the metal ion from a complex formed by the ABC-importer NiuBDE and SlyD.<sup>4,74</sup> It is possible that Ni(II) acquired by this specific uptake pathway is unavailable to UreE<sub>2</sub> until HypA acquires Ni(II) from HypB and performs a handoff to deliver Ni(II) to UreE<sub>2</sub>. However, the very

tight binding of nickel in the HypA•UreE<sub>2</sub> complex would require a specific mechanism to either transfer Ni(II) to UreE<sub>2</sub> and release HypA, or somehow decrease the affinity of the complex so that Ni(II) is available to the urease maturation pathway. It is possible that Ni,Zn-HypA•UreE<sub>2</sub> plays a role in inhibiting nickelation of the large amount of apo-urease present under neutral conditions until the other urease chaperones are ready for correct Ni(II) incorporation. In addition, the HypA•UreE<sub>2</sub> complex might also provide a targeted pool of Ni(II) for rapid urease activation under acid stress, when all the urease apparatus is ready for Ni(II) delivery.

## Conclusions

The results presented here characterize a protein complex formed between HypA and UreE<sub>2</sub> that contains a single high-affinity (sub-nanomolar *K<sub>D</sub>*) Ni(II)-binding site and presumably represents the key interaction between UreE<sub>2</sub> and HypA that is required for maturation of urease in *Hp*. This novel Ni(II) site is located at the intersection of the UreE<sub>2</sub> dimer interface and the rigorously conserved MHE N-terminus of HypA, and is supported by extensive interactions between the component proteins in the absence of Ni(II). The Ni(II) complex is hexa-coordinated and therefore high spin (*S* = 1), and draws on ligands from both component proteins. Direct evidence for the inclusion of the HypA His2 imidazole, Glu3 carboxylate and a pair of His102 imidazole ligands from UreE<sub>2</sub> was obtained from XAS and hyperfine-shifted NMR studies. The addition of the two His ligands from UreE<sub>2</sub> requires substitution of two ligands from the HypA complex. Biochemical studies are most consistent with retention of the N-terminal amine of Met1, suggesting the loss of the Glu3 amide N-donor.<sup>23,25</sup> However, molecular modelling indicates that the N-donors from both His2 and Glu3 are retained, and that the Met1 N-terminal amine present in Ni,Zn-HypA dissociates in forming the Ni,Zn-HypA•UreE<sub>2</sub> complex.

## Supplementary material

Supplementary data are available at [Metallomics](#) online.

## Acknowledgements

Fabio Calogiuri and Massimo Lucci are duly acknowledged for their support in collecting all NMR spectra at CERM—Centre for Magnetic Resonance—University of Firenze, Italy.

## Authors contributions

Protein production was performed by BZ, PB, HH, and VB. Production of HypA containing deuterated Asp or Glu residues was performed by LI and JB. MALS experiments were performed and analyzed by BS and VB. ITC experiments were performed and analyzed by BZ and VB. XAS data collection and analysis was performed by PB. NMR experiments were performed and analyzed by MP. Computation and theoretical studies were performed by FM. Conceptualization was done by MM and SC, who also participated in the final interpretations of the data. All authors contributed to the writing and revisions of the manuscript.

## Funding

The authors acknowledge support for this work from the NIH R01-069696 (M.J.M.). Use of the Stanford Synchrotron Radiation Light-source, SLAC National Accelerator Laboratory, is supported by the

U.S. Department of Energy, Office of Science, Office of Basic Energy Sciences under Contract No. DE-AC02-76SF00515. The SSRL Structural Molecular Biology Program is supported by the DOE Office of Biological and Environmental Research, and by the National Institutes of Health, National Institute of General Medical Sciences (P30GM133894). The contents of this publication are solely the responsibility of the authors and do not necessarily represent the official views of NIGMS or NIH. This work benefited from access to the Cell-Free platform of the Grenoble Instruct-ERIC center (ISBG; UMS 3518 CNRS-CEA-UGA-EMBL), an Instruct-ERIC center, within the Grenoble Partnership for Structural Biology (PSB), supported by FRISBI (ANR-10-INBS-0005-02) and GRAL, financed within the University Grenoble Alpes graduate school (Ecoles Universitaires de Recherche) CBH-EUR-GS (ANR-17-EURE-0003). Financial support was provided by Instruct-ERIC (PID: 13114). VB was supported by a grant from Consorzio Interuniversitario di Risonanze Magnetiche di Metallo-Proteine (CIRMMP). SC, BZ and FM acknowledge partial support by the University of Bologna. MJM was partially supported by the Institute of the Advanced Studies of the University of Bologna through a visiting fellowship.

## Conflict of interest

The authors report no conflicts of interest.

## Data availability

Data and models are available upon request to the authors.

## References

- J. W. Peters, G. J. Schut, E. S. Boyd, D. W. Mulder, E. M. Shepard, J. B. Broderick, P. W. King and M. W. W. Adams, [FeFe]- and [NiFe]-hydrogenase diversity, mechanism, and maturation, *BBA-Mol Cell Res.* 2015, 1853 (12), 1350–1369.
- M. J. Lacasse and D. B. Zamble, [NiFe]-hydrogenase maturation, *Biochemistry* 2016, 55 (12), 1689–1701.
- K. Miki, H. Atomi and S. Watanabe, Structural insight into [NiFe] hydrogenase maturation by transient complexes between Hyp proteins, *Acc. Chem. Res.* 2020, 53 (4), 875–886.
- M. J. Maroney and S. Ciurli, Nickel as a virulence factor in the Class I bacterial carcinogen, *Helicobacter pylori*, *Semin. Cancer Biol.* 2021, 76, 143–155.
- M. Bellucci, B. Zambelli, F. Musiani, P. Turano and S. Ciurli, *Helicobacter pylori* UreE, a urease accessory protein: specific Ni(II)- and Zn(II)-binding properties and interaction with its cognate UreG, *Biochem. J.* 2009, 422 (1), 91–100.
- K. Banaszak, V. Martin-Diaconescu, M. Bellucci, B. Zambelli, W. Rypniewski, M. J. Maroney and S. Ciurli, Crystallographic and X-ray absorption spectroscopic characterization of *Helicobacter pylori* UreE bound to Ni<sup>2+</sup> and Zn<sup>2+</sup> reveals a role for the disordered C-terminal arm in metal trafficking, *Biochem. J.* 2012, 441 (3), 1017–1026.
- A. Merloni, O. Dobrovol'ska, B. Zambelli, F. Agostini, M. Bazzani, F. Musiani and S. Ciurli, Molecular landscape of the interaction between the urease accessory proteins UreE and UreG, *Biochim. Biophys. Acta* 2014, 1844, 1662–1674.
- Y. S. Nim and K.-B. Wong, The maturation pathway of nickel urease, *Inorganics* 2019, 7 (7), 85
- M. Alfano and C. Cavazza, Structure, function, and biosynthesis of nickel-dependent enzymes, *Protein Sci.* 2020, 1–19.
- J. W. Olson, N. S. Mehta and R. J. Maier, Requirement of nickel metabolism proteins HypA and HypB for full activity of both hydrogenase and urease in *Helicobacter pylori*, *Mol. Microbiol.* 2001, 39 (1), 176–182.
- N. Mehta, J. W. Olson and R. J. Maier, Characterization of *Helicobacter pylori* nickel metabolism accessory proteins needed for maturation of both urease and hydrogenase, *J. Bacteriol.* 2003, 185 (3), 726–734.
- S. L. Benoit, N. Mehta, M. V. Weinberg, C. Maier and R. J. Maier, Interaction between the *Helicobacter pylori* accessory proteins HypA and UreE is needed for urease maturation, *Microbiology* 2007, 153 (Pt 5), 1474–1482.
- S. L. Benoit, A. L. Zbell and R. J. Maier, Nickel enzyme maturation in *Helicobacter hepaticus*: roles of accessory proteins in hydrogenase and urease activities, *Microbiology* 2007, 153 (Pt 11), 3748–3756.
- T. L. Testerman and J. Morris, Beyond the stomach: an updated view of *Helicobacter pylori* pathogenesis, diagnosis, and treatment, *World J. Gastroenterol.* 2014, 20 (36), 12781–12808.
- M. Zamani, F. Ebrahimitabar, V. Zamani, W. H. Miller, R. Alizadeh-Navaei, J. Shokri-Shirvani and M. H. Derakhshan, Systematic review with meta-analysis: the worldwide prevalence of *Helicobacter pylori* infection, *Aliment Pharm Therap* 2018, 47 (7), 868–876.
- G. Sachs, D. L. Weeks, Y. Wen, E. A. Marcus, D. R. Scott and K. Melchers, Acid acclimation by *Helicobacter pylori*, *Physiology* 2005, 20, 429–438.
- F. C. Blum, H. Q. Hu, S. L. Servetas, S. L. Benoit, R. J. Maier, M. J. Maroney and D. S. Merrell, Structure-function analyses of metal-binding sites of HypA reveal residues important for hydrogenase maturation in *Helicobacter pylori*, *PLoS One* 2017, 12 (8), e0183260
- G. Wang, J. Romero-Gallo, S. L. Benoit, M. B. Piazuelo, R. L. Dominguez, D. R. Morgan, R. M. Peek, Jr. and R. J. Maier, Hydrogen metabolism in *Helicobacter pylori* plays a role in gastric carcinogenesis through facilitating CagA translocation, *mBio* 2016, 7 (4), e01022–e01016.
- S. L. Benoit, R. J. Maier, R. G. Sawers and C. Greening, Molecular hydrogen metabolism: a widespread trait of pathogenic bacteria and protists, *Microbiol Mol Biol R* 2020, 84 (1), e00092–e00019.
- L. T. Hu and H. L. Mobley, Purification and N-terminal analysis of urease from *Helicobacter pylori*, *Infect. Immun.* 1990, 58 (4), 992–998.
- P. Voland, D. L. Weeks, E. A. Marcus, C. Prinz, G. Sachs and D. Scott, Interactions among the seven *Helicobacter pylori* proteins encoded by the urease gene cluster, *Am. J. Physiol. Gastrointest. Liver Physiol.* 2003, 284 (1), G96–G106.
- R. C. Johnson, H. Q. Hu, D. S. Merrell and M. J. Maroney, Dynamic HypA zinc site is essential for acid viability and proper urease maturation in *Helicobacter pylori*, *Metallomics* 2015, 7 (4), 674–682.
- H. Q. Hu, R. C. Johnson, D. S. Merrell and M. J. Maroney, Nickel ligation of the N-terminal amine of HypA is required for urease maturation in *Helicobacter pylori*, *Biochemistry* 2017, 56 (8), 1105–1116.
- A. Savoldi, E. Carrara, D. Y. Graham, M. Conti and E. Tacconelli, Prevalence of antibiotic resistance in *Helicobacter pylori*: a systematic review and meta-analysis in World Health Organization regions, *Gastroenterology* 2018, 155 (5), 1372–1382. e17
- H. Q. Hu, H. T. Huang and M. J. Maroney, The *Helicobacter pylori* HypA•UreE<sub>2</sub> complex contains a novel high-affinity Ni(II)-binding site, *Biochemistry* 2018, 57, 2932–2942.
- A. C. Rosenzweig, Metallochaperones: bind and deliver, *Chem. Biol.* 2002, 9 (6), 673–677.
- F. Musiani, B. Zambelli, M. Bazzani, L. Mazzei and S. Ciurli, Nickel-responsive transcriptional regulators, *Metallomics* 2015, 7, 1305–1318.

28. B. Zambelli, M. Bellucci, A. Danielli, V. Scarlato and S. Ciurli, The Ni<sup>2+</sup> binding properties of *Helicobacter pylori* NikR, *Chem. Commun. (Camb)* 2007(35), 3649–3651.
29. R. W. Herbst, I. Perovic, V. Martin-Diaconescu, K. O'Brien, P. T. Chivers, S. S. Pochapsky, T. C. Pochapsky and M. J. Maroney, Communication between the zinc and nickel sites in dimeric HypA: metal recognition and pH sensing, *J. Am. Chem. Soc.* 2010, 132 (30), 10338–10351.
30. L. Imbert, R. Lenoir-Capello, E. Crublet, A. Vallet, R. Awad, I. Ayala, C. Juillan-Binard, H. Mayerhofer, R. Kerfah, P. Gans, E. Miclet and J. Boisbouvier, In vitro production of perdeuterated proteins in H<sub>2</sub>O for biomolecular NMR Studies, *Methods Mol. Biol.* 2021, 2199, 127–149.
31. M. Stola, F. Musiani, S. Mangani, P. Turano, N. Safarov, B. Zambelli and S. Ciurli, The nickel site of *Bacillus pasteurii* UreE, a urease metallo-chaperone, as revealed by metal-binding studies and X-ray absorption spectroscopy, *Biochemistry* 2006, 45 (20), 6495–6509.
32. E. Muñoz and A. Piñeiro, AFFINImeter Software: from its beginnings to future trends—A Literature review, *J Appl Bioanal* 2018, 4 (4), 124–139.
33. K. A. Higgins, H. Q. Hu, P. T. Chivers and M. J. Maroney, Effects of select histidine to cysteine mutations on transcriptional regulation by *Escherichia coli* RcnR, *Biochemistry* 2013, 52 (1), 84–97.
34. B. Ravel and M. A. Newville, ARTEMIS, HEPHAESTUS: data analysis for X-ray absorption spectroscopy using IFEFFIT, *J. Synchrotron Radiat.* 2005, 12 (Pt 4), 537–541.
35. V. Martin-Diaconescu and M. J. Maroney, Nickel Bioinorganic Systems, *Comprehensive Inorganic Chemistry II*: Elsevier, 2013, 295–322.
36. F. Delaglio, S. Grzesiek, G. W. Vuister, G. Zhu, J. Pfeifer and A. Bax, NMRPipe: a multidimensional spectral processing system based on UNIX pipes, *J. Biomol. NMR* 1995, 6 (3), 277–293.
37. W. Lee, M. Rahimi, Y. Lee and A. Chiu, POKY: a software suite for multidimensional NMR and 3D structure calculation of biomolecules, *Bioinformatics* 2021
38. M. Piccioli and P. Turano, Transient iron coordination sites in proteins: Exploiting the dual nature of paramagnetic NMR, *Coord. Chem. Rev.* 2015, 284, 313–328.
39. M. Mirdita, K. Schütze, Y. Moriawaki, L. Heo, S. Ovchinnikov and M. Steinegger, ColabFold - Making protein folding accessible to all, *bioRxiv* 2022: 2021.08.15.456425
40. A. W. Senior, R. Evans, J. Jumper, J. Kirkpatrick, L. Sifre, T. Green, C. Qin, A. Zidek, A. W. R. Nelson, A. Bridgland, H. Penedones, S. Petersen, K. Simonyan, S. Crossan, P. Kohli, D. T. Jones, D. Silver, K. Kavukcuoglu and D. Hassabis, Improved protein structure prediction using potentials from deep learning, *Nature* 2020, 577 (7792), 706–710.
41. M. Baek, F. DiMaio, I. Anishchenko, J. Dauparas, S. Ovchinnikov, G. R. Lee, J. Wang, Q. Cong, L. N. Kinch, R. D. Schaeffer, C. Millan, H. Park, C. Adams, C. R. Glassman, A. DeGiovanni, J. H. Pereira, A. V. Rodrigues, A. A. van Dijk, A. C. Ebrecht, D. J. Opperman, T. Sagmeister, C. Buhlheller, T. Pavkov-Keller, M. K. Rathinaswamy, U. Dalwadi, C. K. Yip, J. E. Burke, K. C. Garcia, N. V. Grishin, P. D. Adams, R. J. Read and D. Baker, Accurate prediction of protein structures and interactions using a three-track neural network, *Science* 2021, 373 (6557), 871–876.
42. V. Mariani, M. Biasini, A. Barbato and T. Schwede, IDDT: a local superposition-free score for comparing protein structures and models using distance difference tests, *Bioinformatics* 2013, 29 (21), 2722–2728.
43. V. Martin-Diaconescu, M. Bellucci, F. Musiani, S. Ciurli and M. J. Maroney, Unraveling the *Helicobacter pylori* UreG zinc binding site using X-ray absorption spectroscopy (XAS) and structural modeling, *J. Biol. Inorg. Chem.* 2012, 17 (3), 353–361.
44. C. E. Carr, F. Musiani, H. - T. Huang, P. T. Chivers, S. Ciurli and M. J. Maroney, Glutamate ligation in the Ni(II)- and Co(II)-responsive *Escherichia coli* transcriptional regulator, RcnR, *Inorg. Chem.* 2017, 56 (11), 6459–6476.
45. E. Barchi and F. Musiani, Molecular modelling of the Ni(II)-responsive *Synechocystis* PCC 6803 transcriptional regulator InrS in the metal bound form, *Inorganics* 2019, 7 (6), 76
46. M. A. Martí-Renom, A. C. Stuart, A. Fiser, R. Sánchez, F. Melo and A. Sali, Comparative protein structure modeling of genes and genomes, *Ann. Rev. Biophys. Biomol. Struct.* 2000, 29 (1), 291–325.
47. A. MacKerell, D. Bashford, M. Bellot, R. Dunbrack, J. Evanseck and M. Field, All-atom empirical potential for molecular modeling and dynamics studies of proteins using the CHARMM22 force field, *J. Phys. Chem. B* 1998, 102, 3586–3616.
48. M-y Shen and A. Sali, Statistical potential for assessment and prediction of protein structures, *Protein Sci.* 2006, 15 (11), 2507–2524.
49. R. A. Laskowski, M. W. MacArthur, D. S. Moss and J. M. Thornton, PROCHECK: a program to check the stereochemical quality of protein structures, *J Appl Crystallograph* 1993, 26, 283–291.
50. E. F. Pettersen, T. D. Goddard, C. C. Huang, G. S. Couch, D. M. Greenblatt, E. C. Meng and T. E. Ferrin, UCSF Chimera - A visualization system for exploratory research and analysis, *J. Comput. Chem.* 2004, 25, 1605–1612.
51. T. D. Goddard, C. C. Huang, E. C. Meng, E. F. Pettersen, G. S. Couch, J. H. Morris and T. E. Ferrin, UCSF ChimeraX: Meeting modern challenges in visualization and analysis, *Protein Sci.* 2018, 27 (1), 14–25.
52. E. F. Pettersen, T. D. Goddard, C. C. Huang, E. C. Meng, G. S. Couch, T. I. Croll, J. H. Morris and T. E. Ferrin, UCSF ChimeraX: Structure visualization for researchers, educators, and developers, *Protein Sci.* 2021, 30 (1), 70–82.
53. F. Neese, The ORCA program system, *Wiley Interdiscip Rev: Comput Mol Sci* 2012, 2 (1), 73–78.
54. A. D. Becke, A new mixing of Hartree–Fock and local density-functional theories, *J. Chem. Phys.* 1993, 98 (2), 1372–1377.
55. C. Lee, W. Yang and R. G. Parr, Development of the Colle-Salvetti correlation-energy formula into a functional of the electron density, *Phys. Rev. B* 1988, 37 (2), 785–789.
56. M. J. Frisch, G. W. Trucks, H. B. Schlegel, G. E. Scuseria, M. A. Robb, J. R. Cheeseman, G. Scalmani, V. Barone, B. Mennucci, G. A. Petersson, H. Nakatsuji, M. Caricato, X. Li, H. P. Hratchian, A. F. Izmaylov, J. Bloino, G. Zheng, J. L. Sonnenberg, M. Hada, M. Ehara, K. Toyota, R. Fukuda, J. Hasegawa, M. Ishida, T. Nakajima, Y. Honda, O. Kitao, H. Nakai, T. Vreven, J. A. Montgomery, Jr., J. E. Peralta, F. Ogliaro, M. J. Bearpark, J. Heyd, E. N. Brothers, K. N. Kudin, V. N. Staroverov, R. Kobayashi, J. Normand, K. Raghavachari, A. P. Rendell, J. C. Burant, S. S. Iyengar, J. Tomasi, M. Cossi, N. Rega, N. J. Millam, M. Klene, J. E. Knox, J. B. Cross, V. Bakken, C. Adamo, J. Jaramillo, R. Gomperts, R. E. Stratmann, O. Yazyev, A. J. Austin, R. Cammi, C. Pomelli, J. W. Ochterski, R. L. Martin, K. Morokuma, V. G. Zakrzewski, G. A. Voth, P. Salvador, J. J. Dannenberg, S. Dapprich, A. D. Daniels, Ö. Farkas, J. B. Foresman, J. V. Ortiz, J. Cioslowski and D. J. Fox, *Gaussian 09*. Wallingford, CT, USA: Gaussian, Inc., 2009
57. M. J. Frisch and J. A. Pople, Self-consistent molecular orbital methods 25. Supplementary functions for Gaussian basis sets, *J. Chem. Phys.* 1984, 80, 3265
58. P. J. Hay and W. R. Wadt, Ab initio effective core potentials for molecular calculations. Potentials for K to Au including the outermost core orbitals, *J. Chem. Phys.* 1985, 82 (1), 299–310.

59. X. Yang, H. Li, T. Cheng, W. Xia, Y. T. Lai and H. Sun, Nickel translocation between metallochaperones HypA and UreE in *Helicobacter pylori*, *Metallomics* 2014, 6 (9), 1731–1736.
60. G. J. Colpas, M. J. Maroney, C. Bagyinka, M. Kumar, W. S. Willis, S. L. Suib, N. Baidya and P. K. Mascharak, X-ray spectroscopic studies of nickel complexes, with application to the structure of nickel sites in hydrogenases, *Inorg. Chem.* 1991, 30, 920–928.
61. R. A. Scott, X-Ray Absorption Spectroscopy, In: L. Que, Jr.s (ed), *Physical Methods in Inorganic and Bioinorganic Chemistry*. Menlo Park (CA, USA): University Science Press, 2000
62. C. Spronk, S. Zerko, M. Gorka, W. Kozminski, B. Bardiaux, B. Zambelli, F. Musiani, M. Piccioli, P. Basak, F. C. Blum, R. C. Johnson, H. Hu, D. S. Merrell, M. Maroney and S. Ciurli, Structure and dynamics of *Helicobacter pylori* nickel-chaperone HypA: an integrated approach using NMR spectroscopy, functional assays and computational tools, *J. Biol. Inorg. Chem.* 2018, 23 (8), 1309–1330.
63. W. Xia, H. Li, K.-H. Sze and H. Sun, Structure of a nickel chaperone, HypA, from *Helicobacter pylori* reveals two distinct metal binding sites, *J. Am. Chem. Soc.* 2009, 131 (29), 10031–10040.
64. J. Salgado, A. P. Kalverda, R. E. M. Diederix, G. W. Canters, J.-M. Moratal, A. T. Lawler and C. Dennison, Paramagnetic NMR investigations of Co(II) and Ni(II) amicyanin, *J. Biol. Inorg. Chem.* 1999, 4, 457–467.
65. L. Banci and M. Piccioli, Cobalt(II)- and Nickel(II)-Substituted Proteins, *eMarRes* 2007.
66. B. J. Goodfellow, I. C. Duarte, A. L. Macedo, B. F. Volkman, S. G. Nunes, I. Moura, J. L. Markley and J. J. Moura, An NMR structural study of nickel-substituted rubredoxin, *J. Biol. Inorg. Chem.* 2010, 15 (3), 409–420.
67. S. Ciurli, N. Safarov, S. Miletti, A. Dikiy, S. K. Christensen, K. Kornetzky, D. A. Bryant, I. Vandenberghe, B. Devreese, B. Samyn, H. Remaut and J. Van Beeumen, Molecular characterization of *Bacillus pasteurii* UreE, a metal-binding chaperone for the assembly of the urease active site, *J. Biol. Inorg. Chem.* 2002, 7 (6), 623–631.
68. J. Pereira, A. J. Simpkin, M. D. Hartmann, D. J. Rigden, R. M. Keegan and A. N. Lupas, High-accuracy protein structure prediction in CASP14, *Proteins* 2021, 89 (12), 1687–1699.
69. G. Camporesi, A. Minzoni, L. Morasso, S. Ciurli and F. Musiani, Nickel import and export in the human pathogen *Helicobacter pylori*, perspectives from molecular modelling, *Metallomics* 2021, 13 (12).
70. L. Mazzei, F. Musiani and C. S. Urease D Zamble, M. Rowińska-Zyrek Hs Kozłowski (eds). *The Biological Chemistry of Nickel*. London, UK: Royal Society of Chemistry, 2017, 60–97.
71. X. Yang, H. Li, T. P. Lai and H. Sun, UreE-UreG complex facilitates nickel transfer and preactivates GTPase of UreG in *Helicobacter pylori*, *J. Biol. Chem.* 2015, 290, 12474–12485.
72. A. Soriano and R. P. Hausinger, GTP-dependent activation of urease apoprotein in complex with the UreD, UreF, and UreG accessory proteins, *Proc Natl Acad Sci, USA* 1999, 96 (20), 11140–11144.
73. Y. H. Fong, H. C. Wong, M. H. Yuen, P. H. Lau, Y. W. Chen and K. B. Wong, Structure of UreG/UreF/UreH complex reveals how urease accessory proteins facilitate maturation of *Helicobacter pylori* urease, *PLoS Biol.* 2013, 11 (10), e1001678.
74. M. Denic, E. Turlin, V. Michel, F. Fischer, M. Khorasani-Motlagh, D. Zamble, D. Vinella and H. de Reuse, A novel mode of control of nickel uptake by a multifunctional metallochaperone, *PLoS Pathog.* 2021, 17 (1), e1009193.